Trust & Quality

Inspecta

INSPECTA

TECHNICAL REPORT

SKB

Defect distributions for BWR- and PWR-insert material

Report No.: 50017480-1

Revision No.: 2

INSPECTA TECHNOLOGY AB

BOX 30100 104 25 STOCKHOLM TEL 08-5011 3000 FAX 08-5011 3001 www.inspecta.com

Date	Our project No.
2014-02-27	50017480
Approved by	Organizational unit
Keivan Ashhami	Inspecta Technology AB
Customer	Customer reference
SKB	Mikael Jonsson

Summary

In this report, defect distributions are developed and documented, for both BWR- and PWR-inserts. These distributions can be used in a probabilistic analysis.

There is a distinct difference between the crack-like defects that are found in BWR- and PWR-inserts. The defects found in PWR-inserts are much smaller (mean value = 0.8 mm) than the defects found in BWR-inserts (mean value = 1.2 mm). Also, there are no outliers in the data set from the PWR-inserts.

An analysis was performed to check whether the assumption, that the found defects are to be treated as crack-like defects, is pessimistic or not. The analysis showed that when it is a good agreement between the analyzed defect and the real defect then the assumption of a crack like defect seems to be valid. However, when it is a large difference between the analyzed defect and the real defect then the assumption of a crack like defect seems to be very pessimistic.

Report title	
Defect distributions for BWR- and PWR-insert material	Index terms —
Work carried out by Peter Dillström, Lars Alverlind	Distribution
Work verified by Andrey Shipsha	☒ No distribution without permission from the customer or Inspecta Technology AB. ☐ Limited distribution in Inspecta Technology AB. ☐ Unrestricted distribution.

Table of content ***Page***

1 INTRODUCTION

The purpose of this report is to develop and document defect distributions, for BWR- and PWR-inserts, that can be used in a probabilistic analysis. It is also of interest to have some knowledge about what kind of defects that can be found in the inserts. Finally, an analysis is performed to check whether the assumption, that the found defects are to be treated as crack-like defects, is conservative or not.

2 DEFECT DISTRIBUTIONS OF CRACK-LIKE DEFECTS

In general, defect depth distributions are quite difficult to estimate reliably for any given application. Also, using modern ultrasonic and destructive inspection techniques shows a significantly higher probability of small defects and lower probability of larger defects [1] as compared to commonly used defect distributions. In order to get a good estimate of a defect distribution it is best to use some kind of destructive technique. SKB has therefore conducted an extensive fractographic and metallographic study on broken test specimens to check for defects. This data, in the form of defect depth distributions, are going to be used in a probabilistic analysis of canister inserts for spent nuclear fuel in the case of an earthquake induced rock shear load [2].

2.1 Data from fracture surfaces on broken test specimens

SKB has, over the years, performed many tensile (and compression) tests of the different inserts. SKB has also conducted an extensive fractographic and metallographic study on broken test specimens to check for defects. The test series conducted in 2003-2004, which was used in the probabilistic analysis with an isostatic pressure load [3], are not characteristic of the inserts today. More recent tests show that the number of large defects has been reduced considerably. SKB decided to perform a new investigation using fracture surfaces on broken tensile test specimens of both BWR- and PWR-inserts. These defect data are used to develop new defect distributions that more realistically reflects the insert material of today.

The purpose of this investigation is the analysis of defects which are located at the fracture surface of the tensile test specimens that has been taken from both BWR- and PWR-inserts. In this work, the area of each defect shall be accurately estimated (see Fig. 2-1). Furthermore an ellipse will be drawn surrounding the detected defect or cluster of defects (see Fig. 2-1) and the major and minor axis of the ellipse are measured.

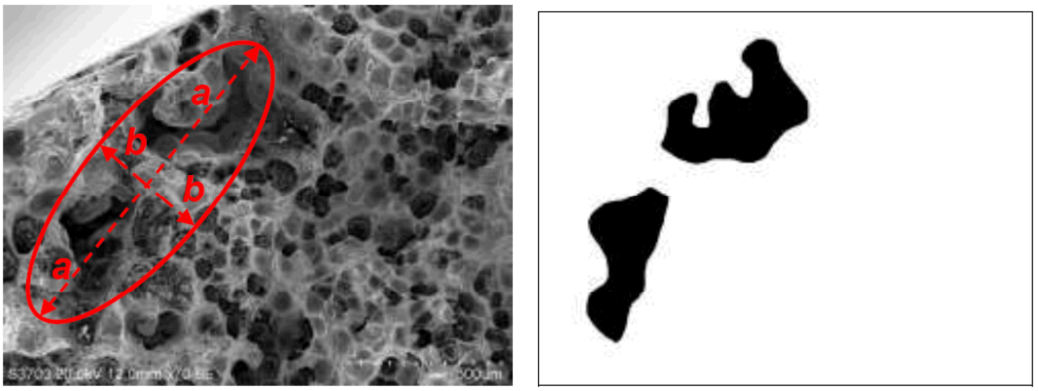

Figure 2-1. Example of an investigation of a defect that is located at the fracture surface, defect area (the right figure) and drawn ellipse (the left figure).

2.2 Assumption regarding crack-like defects

After a defect has been measured, the type of defect is identified as being either porosity defects or graphite/dross defects [4-6]. In the study presented in this report, porosity defects were not considered to be crack-like defects. However, graphite/dross defects were considered to be crack-like defects. To check these assumptions the size of porosity defects (given as total defect area) was plotted against the elongation at fracture for the test specimens where porosity defects were found on the fracture surface (Figure 2-2). Also, the size of graphite/dross defects (given as total defect area) was plotted against the elongation at fracture for the test specimens where graphite/dross defects were found on the fracture surface (Figure 2-2). The data are taken from section 3 (defects found in test specimens taken from BWR-inserts [4-6]).

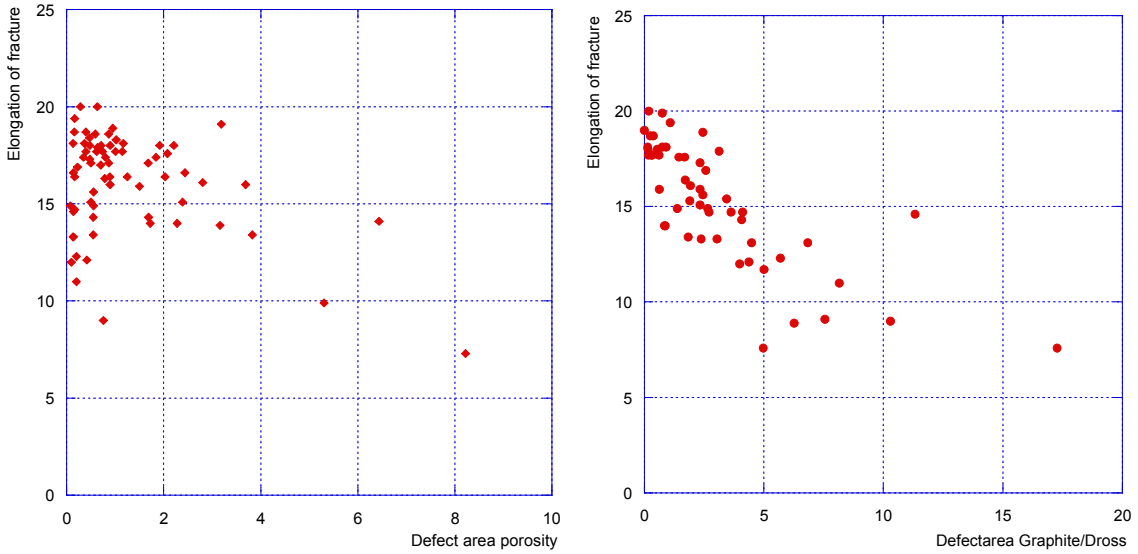

Figure 2-2. Total defect area [mm^2] for porosity defects and graphite/dross defects plotted against the elongation at fracture.

As can be seen in Figure 2-2, the area for porosity defects has a weak correlation against the elongation at fracture. The area for graphite/dross defects has a much better correlation against the elongation at fracture. This indicates that graphite/dross defects should be included when developing a new defect distribution for crack-like defects. This type of defect was also considered relevant when a defect distribution was developed for the probabilistic analysis with an isostatic pressure load [3].

In the probabilistic analysis we are going to assume the existence of one crack-like defect, and the size (depth) of this defect is then characterized by a defect depth distribution. In order to simplify the analysis we assume that the defect is surface breaking, which is more severe than a subsurface defect and therefore conservative.

To develop a defect depth distribution for surface breaking defects, the major and minor axis of the ellipse (drawn surrounding the real defect, see Fig. 2-1) are going to be used. A realistic assumption is to use the minor axis of the ellipse to be the defect depth and the major axis to be the defect length (at the surface). Another possibility is to use the major axis to be the defect depth and an equivalent length over depth ratio of the defect. This is clearly too conservative as can be seen in Fig. 2-3.

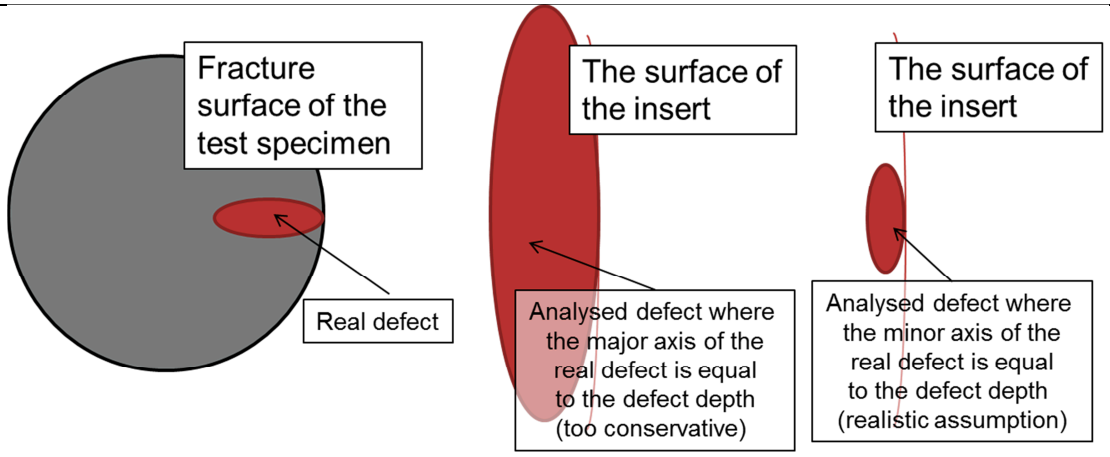

Figure 2-3. Assumption regarding the relation between the real defect and the defect that are used to define the defect distribution.

3 DEFECT DISTRIBUTION FOR BWR-INSERTS

In order to develop a defect depth distribution for BWR-inserts, fracture surfaces on broken tensile test specimens of the inserts I53, I54, I55, I56, and I57 [4-6] were investigated. On each fracture surface, and for each defect found on that surface, the following information was summarized:

- Test specimen number.
- Type of defect (porosity defects and graphite/dross defects) on that surface. The graphite/dross defects should be included when developing a new defect distribution for crack-like defects.
- Area of defect (the real defect was first manually marked by using a photo manipulation tool and then an image analysis software was used to measure the exact area of the defect, see Fig. 2-1).
- Area of ellipse (drawn surrounding the real defect, see Fig. 2-1).
- Major and minor axis of the ellipse (see Fig. 2-1). The minor axis of the ellipse is equal to the defect depth and the major axis is equal to the defect length.

The data, from BWR-inserts I53, I54, I55, I56, and I57 [4-6], is summarized in Appendix A.

As can be seen in Appendix A, 100 defects were found on the fracture surfaces of 90 tensile test specimens. To visualize the data, a dot plot is presented in Fig. 3-1. A dot plot is an easy way to quickly examine a variable and extract its major characteristics. A dot plot can also help detect any unusual observations (outliers), or any gaps in the data set.

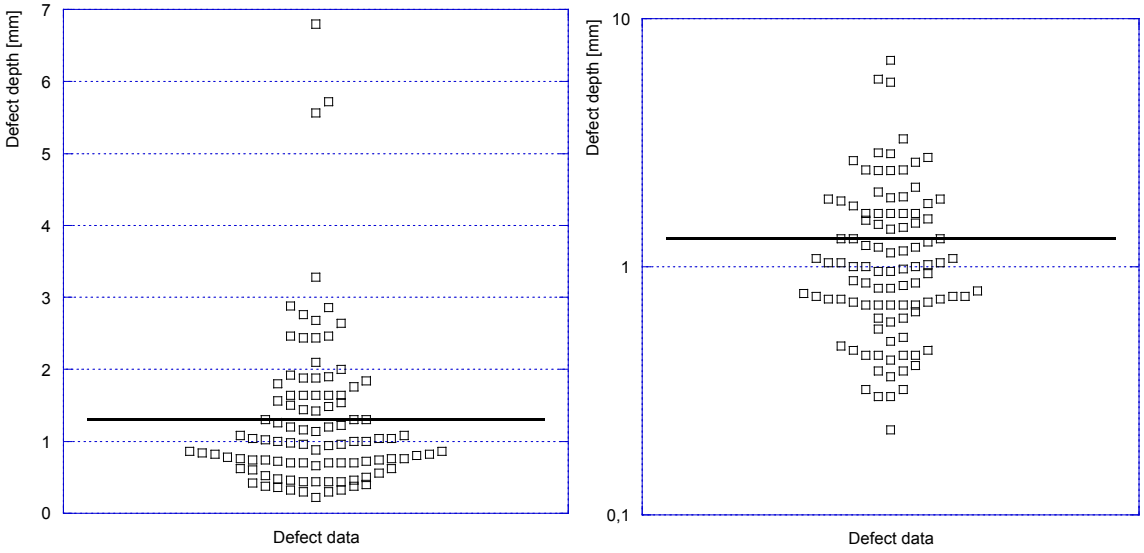

Figure 3-1. Dot plot of the 100 defects that were found on the fracture surfaces of 90 BWR insert tensile test specimens (linear and logarithmic scale).

As can be seen from Fig. 3-1, most of the defect depth data are concentrated just below a depth value of 1 mm. Three data points are larger than the rest of the data and one data point is smaller than the rest of the data.

Another way to visualize the data is to use a probability plot that gives rough information about the local density of the data and symmetry. Such a plot is presented in Fig. 3-2.

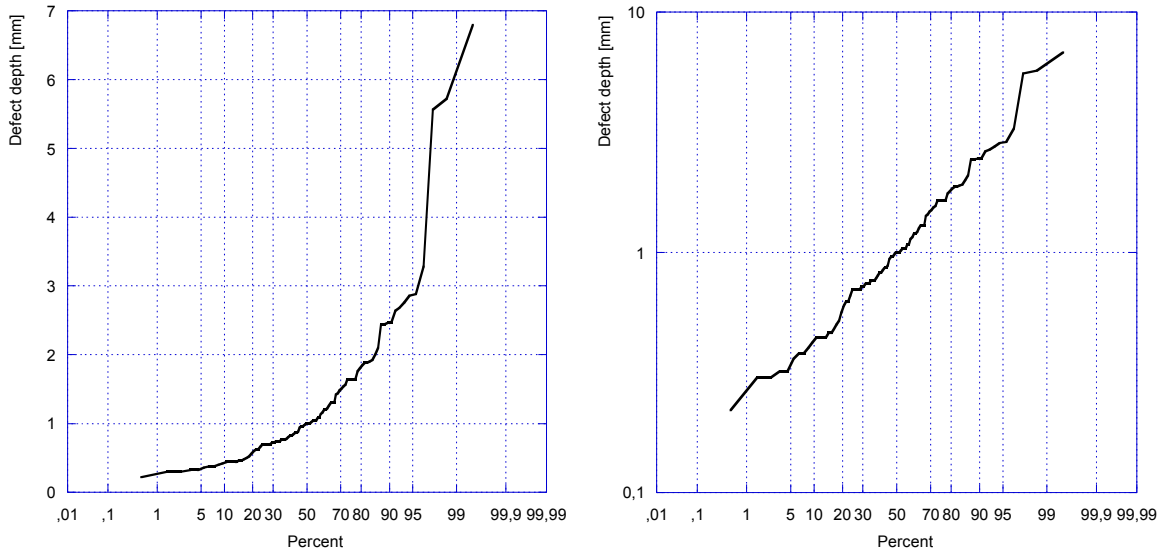

Figure 3-2. Probability plot of the 100 defects that were found on the fracture surfaces of 90 BWR insert tensile test specimens (linear and logarithmic scale).

As can be seen in Fig 3-2, using a logarithmic scale, the defect depth data will probably have a good fit to a lognormal distribution. However, the defect depth distributions most often used are the exponential, lognormal and Weibull distributions [1]. The distribution, most commonly used within the nuclear industry (for thick walled components), is the exponential distribution [1]. A fit to an exponential and lognormal distribution is presented in Fig. 3-3 to 3-4.

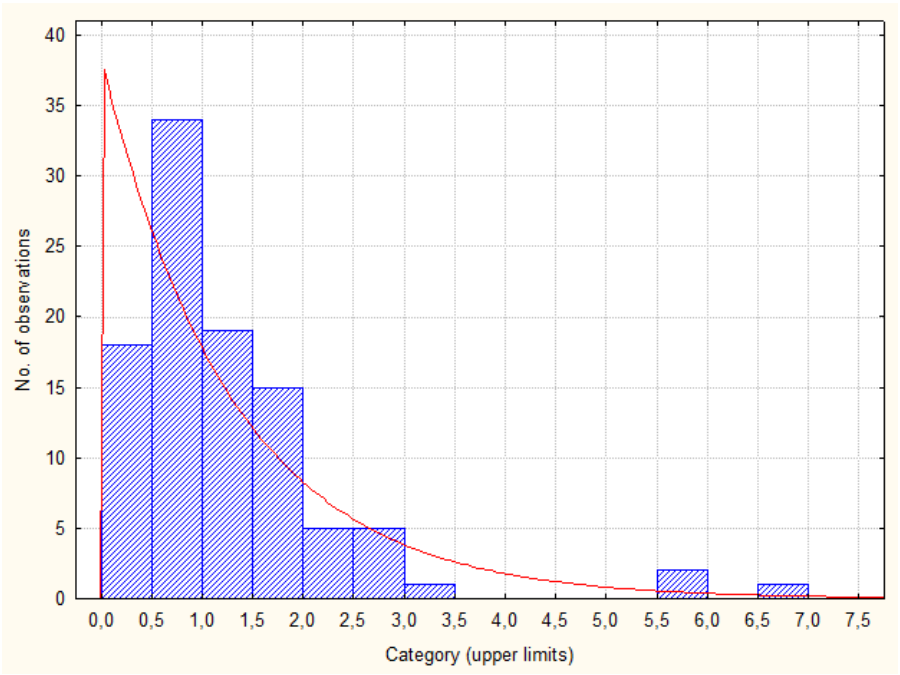

Figure 3-3. Defect depth data [mm] and a fit to an exponential distribution (BWR inserts).

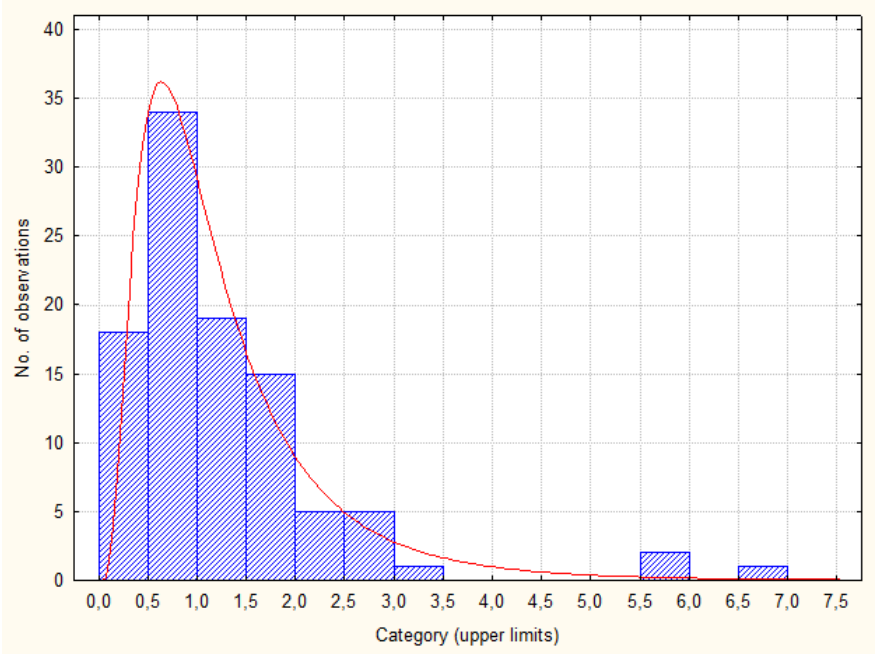

Figure 3-4. Defect depth data [mm] and a fit to a lognormal distribution (BWR inserts).

The choice of defect depth distribution is quite important when performing a probabilistic analysis; therefore a sensitivity analysis should be performed using an exponential, lognormal or a Weibull defect depth distribution (as recommended in [1]). A comparison between the three distributions is shown in Fig. 3-5 to 3-6.

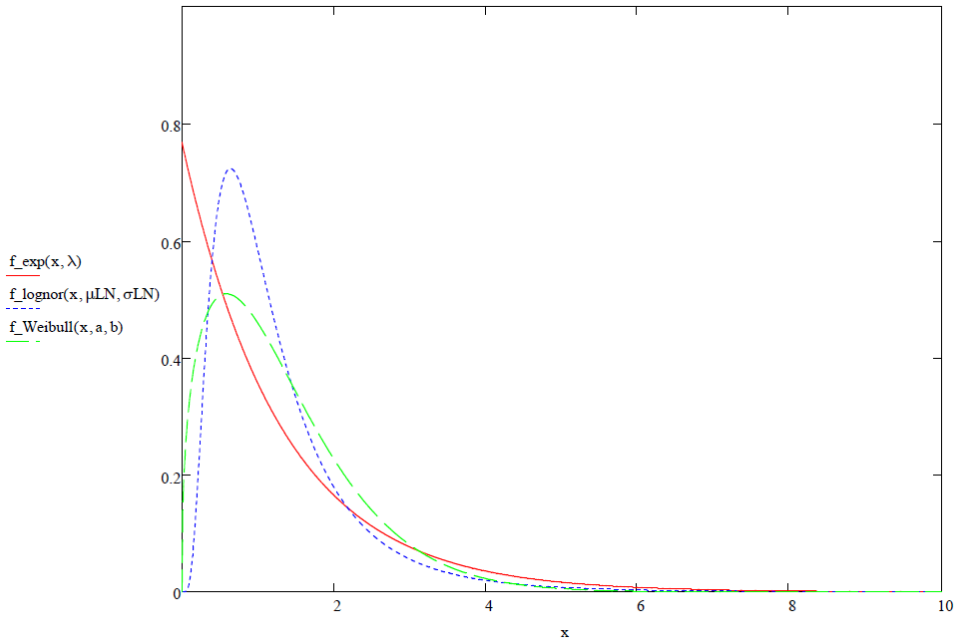

Figure 3-5. Comparison between an exponential, lognormal and Weibull defect depth [mm] distribution (linear scale).

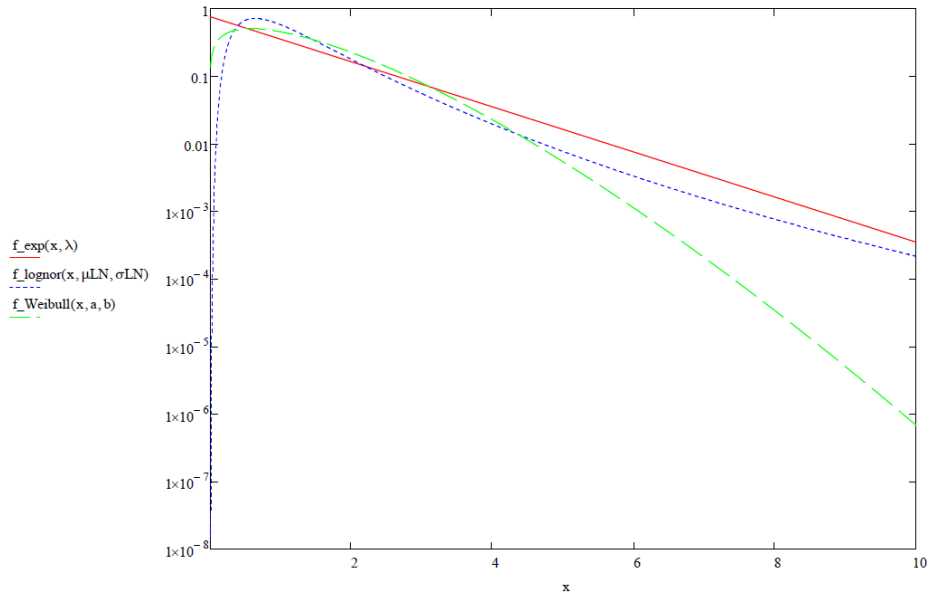

Figure 3-6. Comparison between an exponential, lognormal and Weibull defect depth [mm] distribution (logarithmic scale).

As can be seen in Fig. 3-5 to 3-6, for defects larger than ~1 mm (depth) there is only a minor difference between the exponential and lognormal distribution (but a major difference for defects smaller than ~1 mm). The largest difference between the Weibull distribution and the others are that the Weibull distribution differs for defects larger than ~6 mm. However, in practice, the Weibull distribution is seldom used to model crack-like defects in materials that does not behave in a brittle manner.

Finally, it could be of interest to compare the defect frequency (from data) with the probability to have defects which are larger than a specific defect depth using the three distributions (see Fig. 3-7). As before, the Weibull distribution is below the other distributions and the actual data follows more closely the exponential and lognormal distribution.

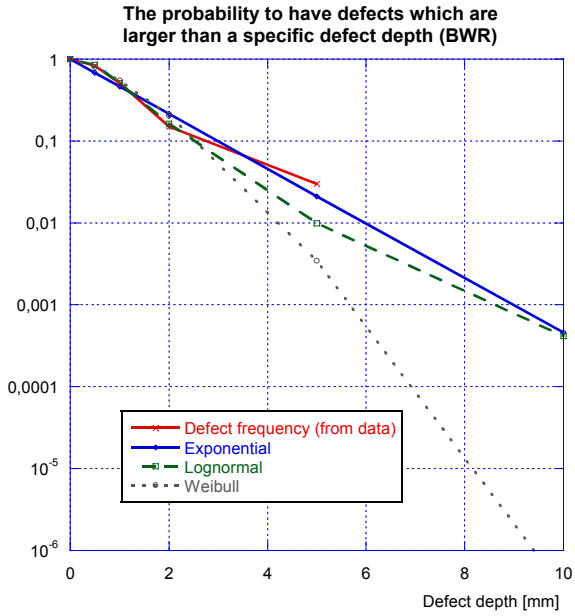

Figure 3-7. Comparison between the defect frequency (from BWR-data) with the probability to have defects which are larger than a specific defect depth (using different distributions).

When fitting the data to the different distributions there are some differences in the calculated mean values and standard deviation (see Table 3-1).

Table 3-1. Comparison between an exponential, lognormal and Weibull defect depth [mm] distribution.

Distribution	Mean	Std Dev
Exponential	1.30	1.30
Lognormal	1.29	0.99
Weibull	1.32	0.95

In the probabilistic analysis we are going to assume the existence of one crack-like defect, and the size (depth) of this defect is characterized by an exponential distribution (same assumption as in the earlier study [3] and most often used for thick walled components [1]).

4 DEFECT DISTRIBUTION FOR BWR-INSERTS USING CORRECTED DATA

The data presented in section 3 was used in the probabilistic analysis of BWR canister inserts for spent nuclear fuel in the case of an earthquake induced rock shear load [2]. After this analysis was finalized a correction was made to the measured defect data from the fracture surfaces on broken tensile test specimens of the inserts I53, I54, I55, I56, and I57. Below, new defect distributions are presented using this corrected data [7-9]. The corrected data is also summarized in Appendix B.

To visualize and compare the data sets, a dot plot is presented in Fig. 4-1. A dot plot is an easy way to quickly examine a variable and extract its major characteristics. A dot plot can also help detect any unusual observations (outliers), or any gaps in the data set.

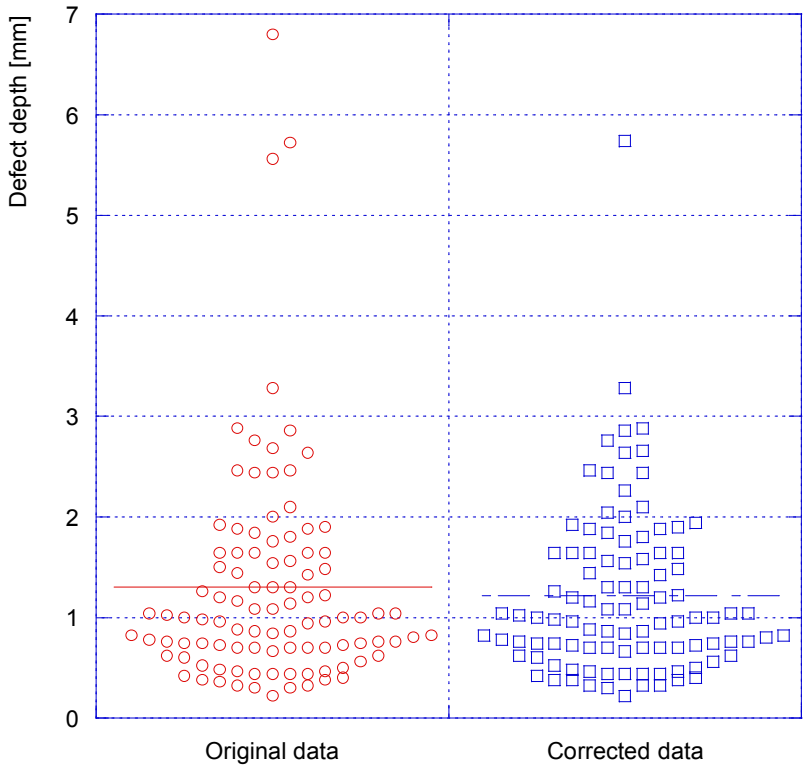

Figure 4-1. Dot plot of the 100 defects that were found on the fracture surfaces of 90 BWR insert tensile test specimens (a comparison between the defect depth data from section 3 and the corrected data).

Obviously, in the corrected data set, two of the largest defect depth values have been corrected and therefore the mean value and standard deviation will be smaller in the new data set. A new data fit was performed using the exponential, lognormal and Weibull defect depth distribution (see Table 4-1).

Table 4-1. Comparison between an exponential, lognormal and Weibull defect depth [mm] distribution.

Distribution	Mean	Std Dev
Exponential	1.22	1.22
Lognormal	1.22	0.87
Weibull	1.23	0.78

The analysis shows that the mean values decrease between 5-7%. The difference is larger for the standard deviation values, which decrease between 6-18%. The largest difference is found when using a Weibull defect depth distribution.

5 DEFECT DISTRIBUTION FOR PWR-INSERTS

In order to develop a defect depth distribution for PWR-inserts, fracture surfaces on broken tensile test specimens of the inserts IP23, IP24 and IP25 [10-12] were investigated. On each fracture surface, and for each defect found on that surface, the following information was summarized:

- Test specimen number.
- Type of defect (porosity defects and graphite/dross defects) on that surface. The graphite/dross defects should be included when developing a new defect distribution for crack-like defects (using the same assumptions as given for defect data from BWR-inserts, see Sect. 2.2).
- Area of defect (the real defect was first manually marked by using a photo manipulation tool and then an image analysis software was used to measure the exact area of the defect, see Fig. 2-1).
- Area of ellipse (drawn surrounding the real defect, see Fig. 2-1).
- Major and minor axis of the ellipse (see Fig. 2-1). The minor axis of the ellipse is equal to the defect depth and the major axis is equal to the defect length.

The data, from PWR-inserts IP23, IP24 and IP25 [10-12], is summarized in Appendix C.

As can be seen in Appendix C, 40 defects were found on the fracture surfaces of 72 tensile test specimens. To visualize the data, a dot plot is presented in Fig. 5-1.

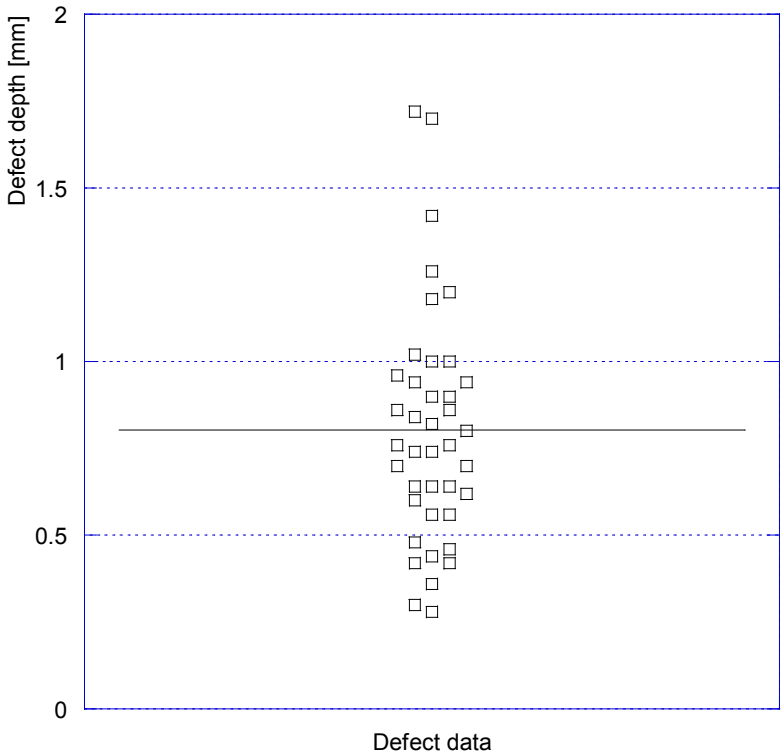

Figure 5-1. Dot plot of the 40 defects that were found on the fracture surfaces of 72 PWR insert tensile test specimens.

As can be seen from Fig. 5-1, most of the defect depth data are concentrated around a mean value of 0.8 mm. There are no significant outliers in the data set.

Another way to visualize the data is to use a probability plot that gives rough information about the local density of the data and symmetry. Such a plot is presented in Fig. 5-2.

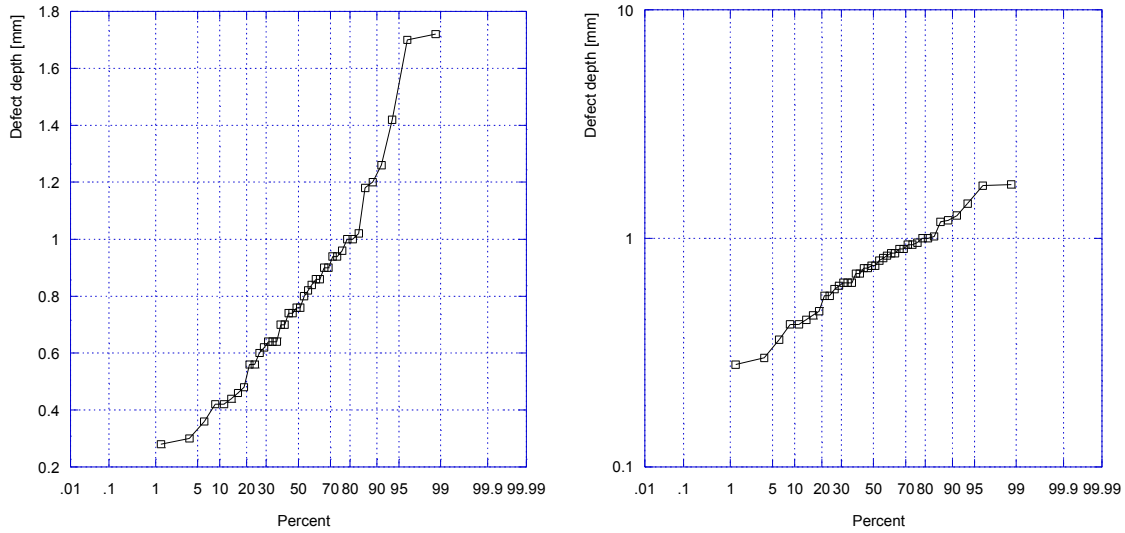

Figure 5-2. Probability plot of the 40 defects that were found on the fracture surfaces of 72 PWR insert tensile test specimens (linear and logarithmic scale).

As can be seen in Fig 5-2, using a logarithmic scale, the defect depth data will probably have a good fit to a lognormal distribution. A fit to an exponential and lognormal distribution is presented in Fig. 5-3 to 5-4.

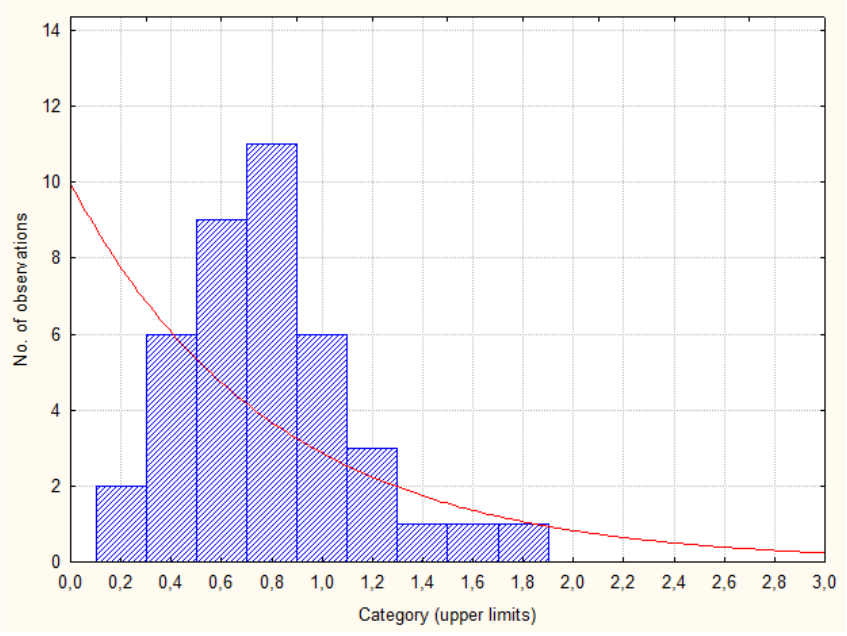

Figure 5-3. Defect depth data [mm] and a fit to an exponential distribution (PWR inserts).

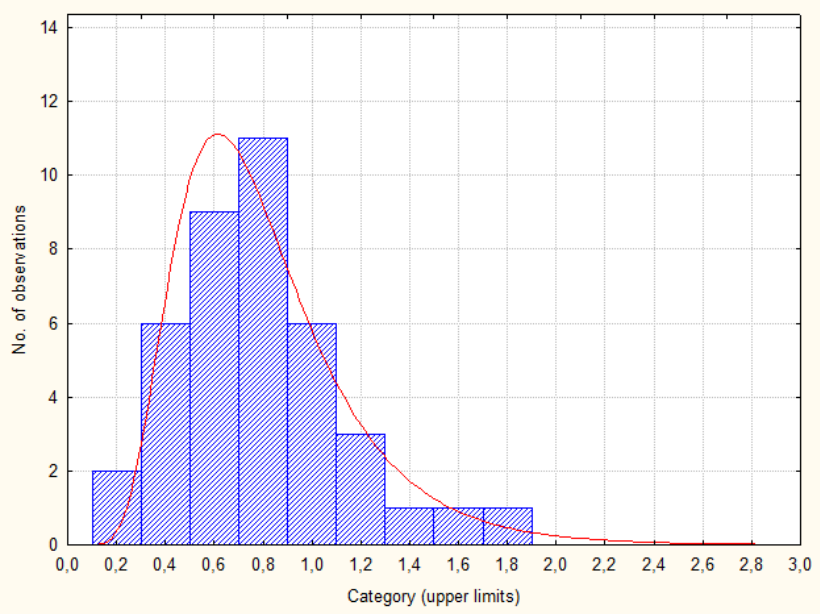

Figure 5-4. Defect depth data [mm] and a fit to a lognormal distribution (PWR inserts).

A lognormal distribution gives a much better fit to the data. As mentioned earlier, the choice of defect depth distribution is quite important when performing a probabilistic analysis; therefore a sensitivity analysis should be performed using an exponential, lognormal or a Weibull defect depth distribution. A comparison between the three distributions is shown in Fig. 5-5 to 5-6.

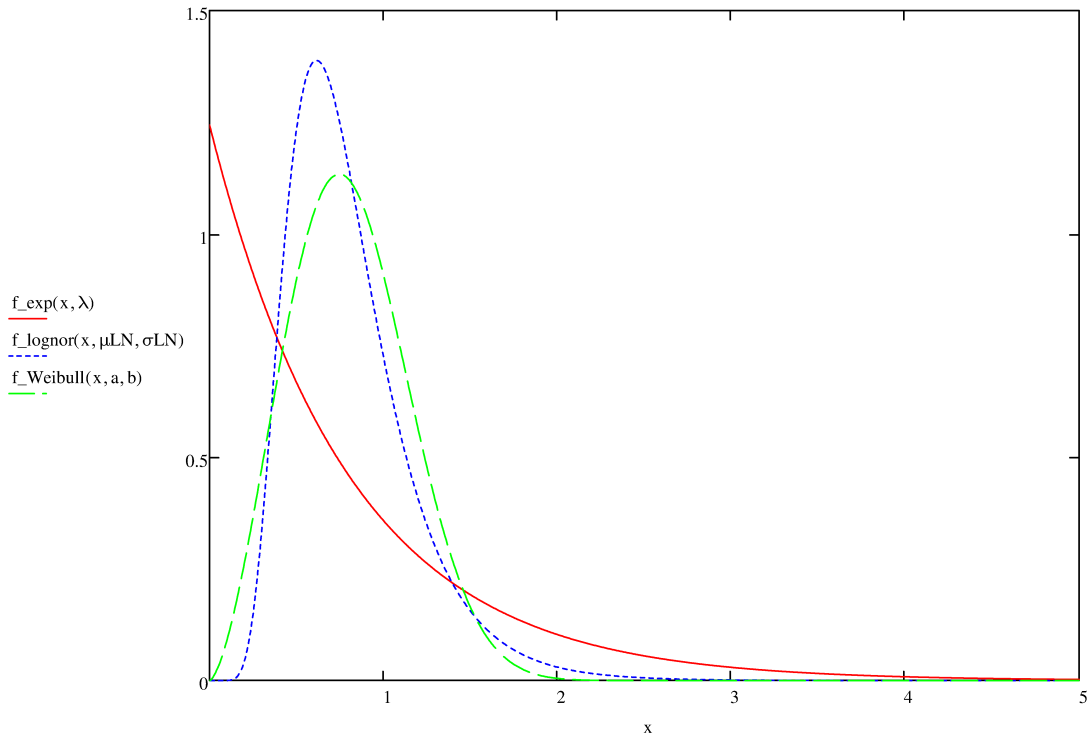

Figure 5-5. Comparison between an exponential, lognormal and Weibull defect depth [mm] distribution (linear scale).

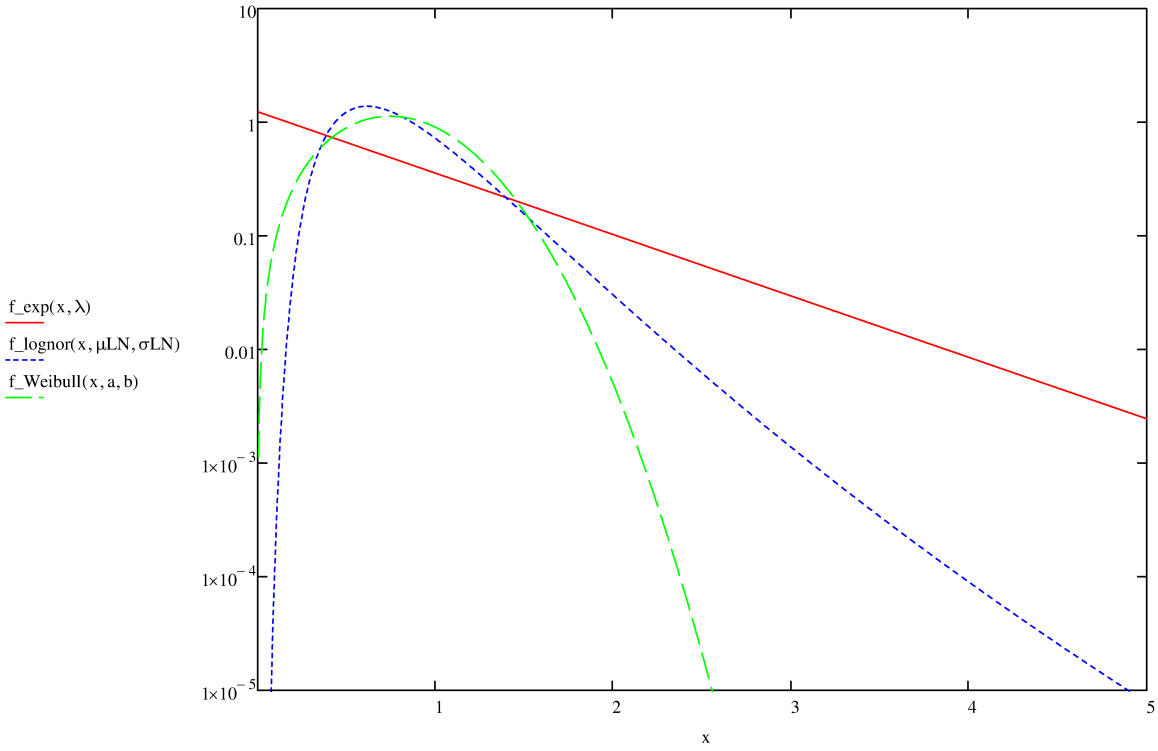

Figure 5-6. Comparison between an exponential, lognormal and Weibull defect depth [mm] distribution (logarithmic scale).

As can be seen in Fig. 5-5 to 5-6, there is quite a large difference between the three distributions.

Finally, it could be of interest to compare the defect frequency (from data) with the probability to have defects which are larger than a specific defect depth using the three distributions (see Fig. 5-7). As can be seen, the actual data follows more closely the lognormal distribution.

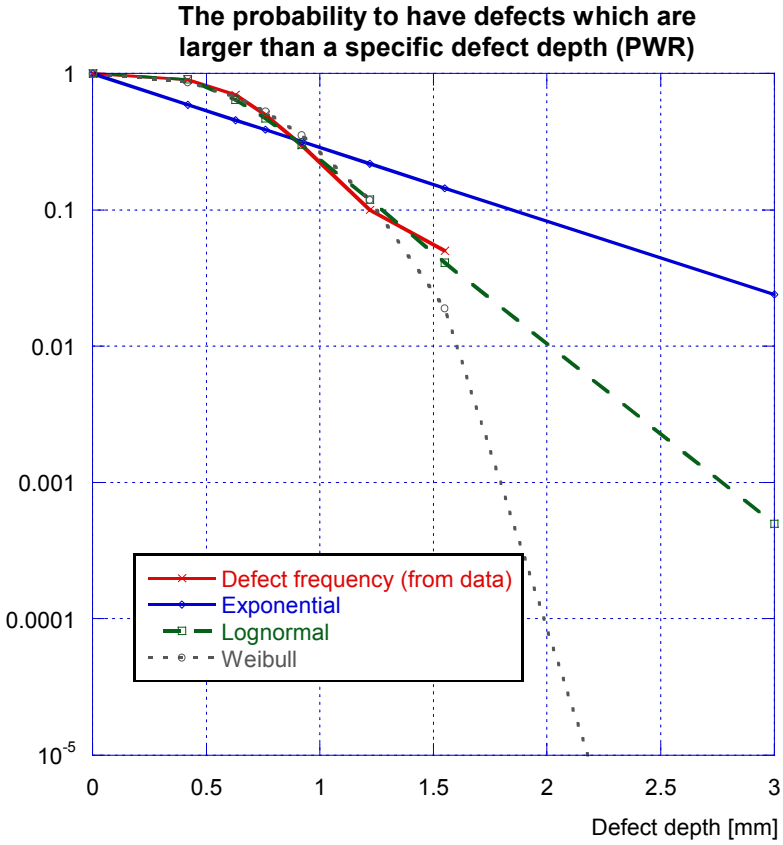

Figure 5-7. Comparison between the defect frequency (from PWR-data) with the probability to have defects which are larger than a specific defect depth (using different distributions).

When fitting the data to the different distributions there are some differences in the calculated mean values and standard deviation (see Table 5-1).

Table 5-1. Comparison between an exponential, lognormal and Weibull defect depth [mm] distribution.

Distribution	Mean	Std Dev
Exponential	0.80	0.80
Lognormal	0.81	0.36
Weibull	0.80	0.34

6 COMPARISON BETWEEN TENSILE TESTS AND FE-ANALYSIS

In this section, several FE-analyses are performed to check whether the assumption, that the found defects are to be treated as crack-like defects, is conservative or not. In order to check this assumption two defects in two different tensile test specimen were chosen to be analyzed (see Fig. 6-1 to 6-2). A summary of the chosen test specimens and defects can be found in Table 6-1.

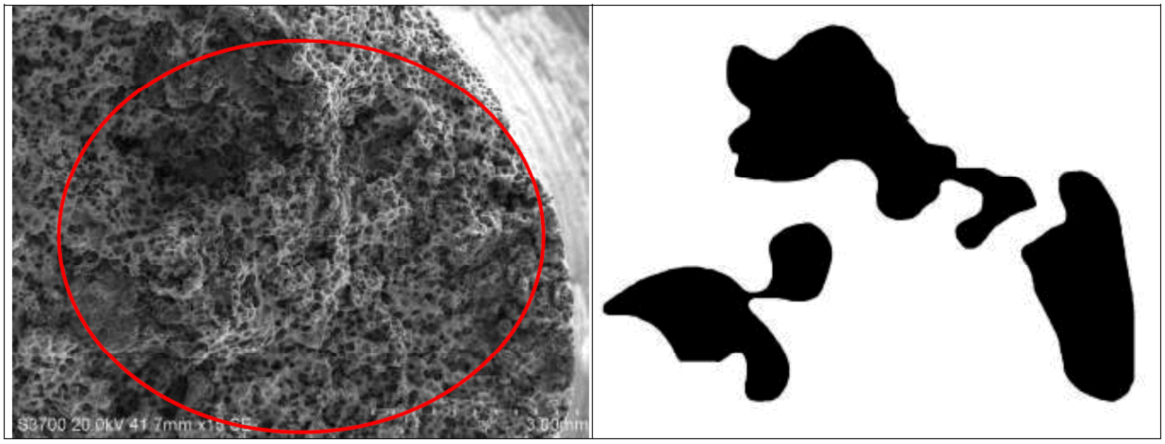

Figure 6-1. A very large defect taken from tensile test specimen I54T [7].

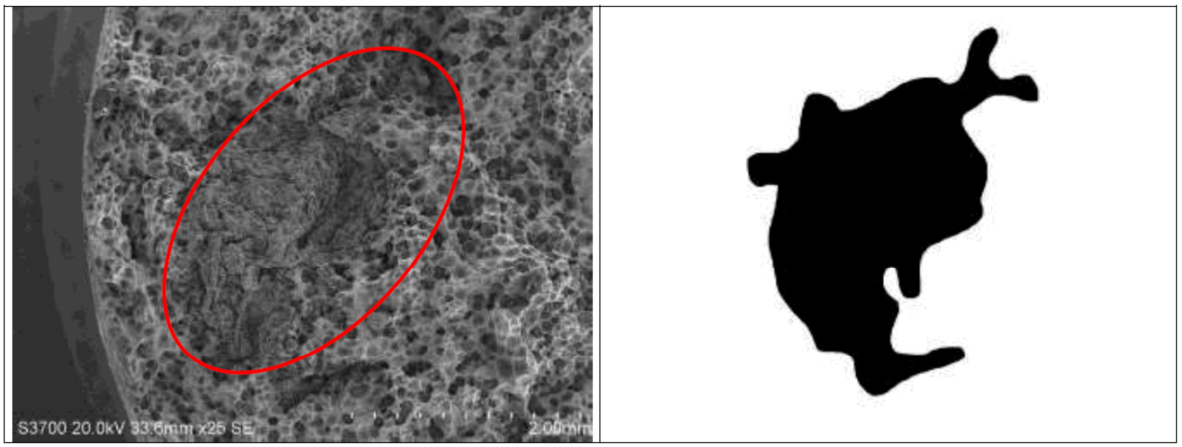

Figure 6-2. Medium size defect taken from tensile test specimen I56T [7].

Table 6-1. A summary of the chosen test specimen and defect data [7].

Defect	From test specimen	Defects area [mm^2]	Ellipse area [mm^2]	Major axis [mm]	Minor axis [mm]	Elongation at fracture
1	I54T	15.84	31.95	7.1	5.74	9
2	I56T	4.94	5.09	3.34	1.94	13.1

As can be seen above, the medium sized defect 2 has a surrounding ellipse that closely resembles the real defect (the difference between the area of the ellipse and the real defect is +4%). On the other hand, the large defect 1 has a surrounding ellipse that doesn't resembles the real defect since the ellipse encloses three minor defects (the difference between the area of the ellipse and the real defect is +102%). This indicates that defect 1 is very conservative and defect 2 should behave like a crack-like defect. To check this, a FE-analysis that simulates the tensile test is performed. In the FE-model cracks are introduced to be able to calculate *J*-values which should be compared to fracture toughness values at initiation of crack growth and 2 mm stable crack growth.

6.1 Modelling of the tensile test specimens

6.1.1 Insert material data

The material in the analysis is described by a multi-linear elastic plastic model (see Table 6-2). The elastic modulus is 166 GPa with a Poisson coefficient of 0.32.

Table 6-2. Stress/strain-curve for the BWR insert material [2].

True strain (%)	True stress [MPa]
0	0
0.169	280.4
1.98	322.6
3.92	361
5.83	392.3
7.7	414.6
9.53	431.5
12.1	448.8

6.1.2 Finite element model

The test specimens are modelled in Abaqus 6.10. The desired crack depth and length are input to create a cylinder around the crack front mapped mesh with C3D20 elements where the *J*-integral is calculated during loading. The rest of the specimen is free meshed with C3D10 elements. The modelled length of the test specimen is 100 mm and the diameter is 14 mm.

The modelling of the crack dimensions is presented in Fig. 6-3, where the cross section of the specimen and the crack surface is shown. The crack is modelled as an elliptical surface crack and the length and depth measurements have the same definitions as if the crack had been a surface crack in a plate. This means that the length dimensions is not a measurement of the crack length along the surface but rather the length of the crack fronts elongation to an axis orthogonal to the depth axis (see Fig. 6-3, that shows the definition of the crack length).

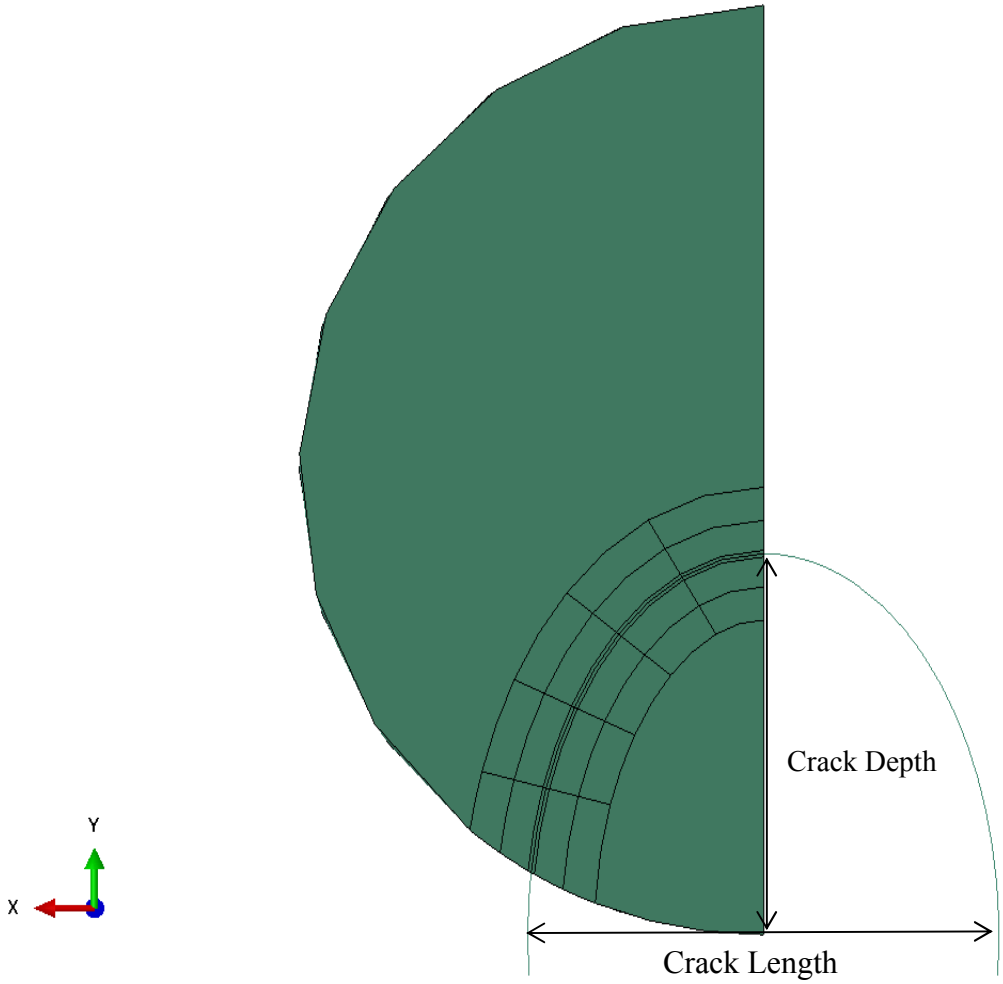

Figure 6-3. The modelling of an elliptical surface crack.

6.1.3 Symmetry and boundary conditions

Symmetry is used to only model and analyze one quarter of the test specimen. This is accomplished by an axial displacement constraint on the cross section of the specimen at the uncracked ligament, and the symmetry surface seen in figure 6-4.

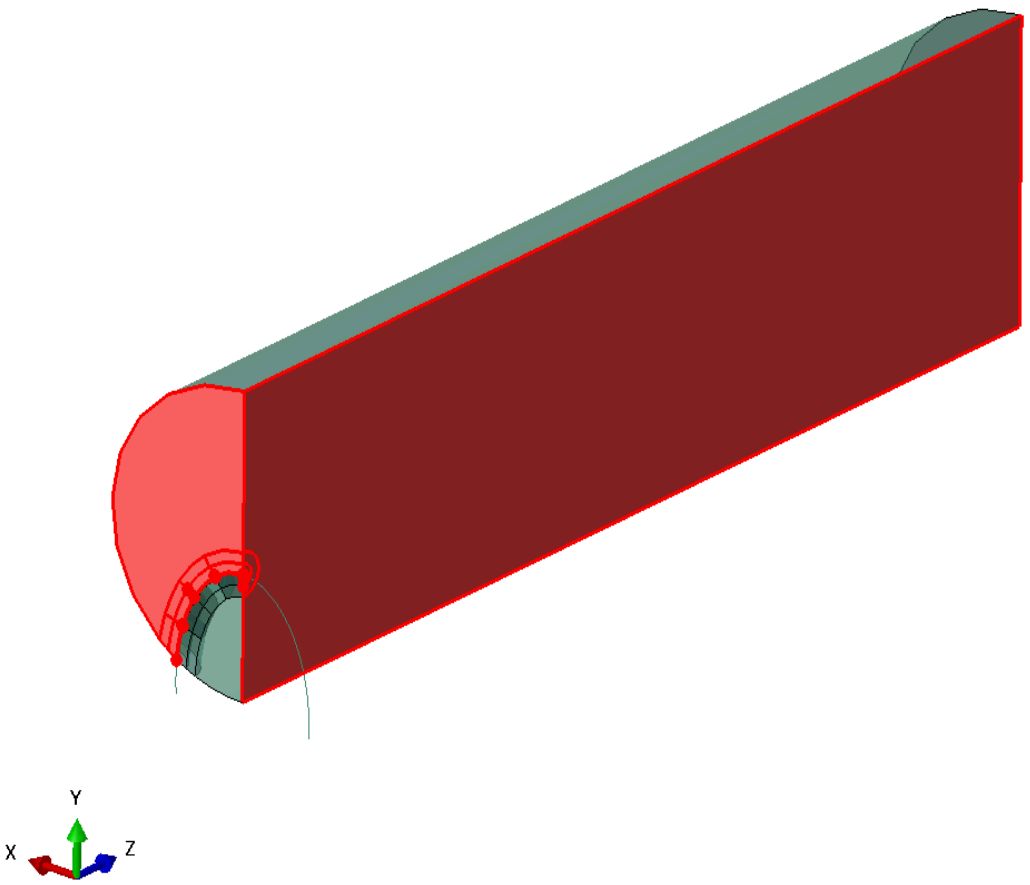

Figure 6-4. Symmetry and boundary conditions.

6.1.4 Applied displacement load

Load is applied to the FE-model as prescribed displacement of the specimen cross section opposite the cracked cross section. Displacement is incrementally applied in the axial direction (Z-direction in Fig. 6-5). Max displacement is 5 mm, equivalent to 10% engineering strain.

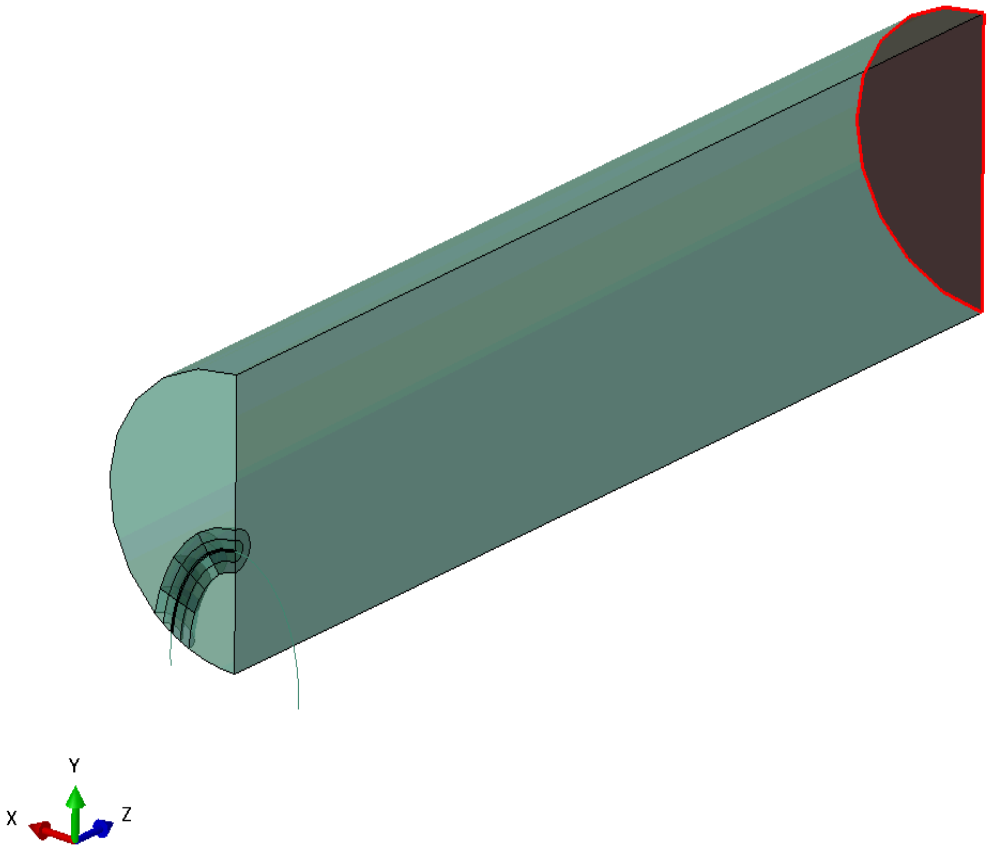

Figure 6-5. Surface where displacement load is applied.

6.2 Results from the FE-simulation of the tensile tests

J-integral values are evaluated during all stages of the simulated tensile test (the crack fronts are shown in Fig. 6-6). The engineering strain is calculated as the ratio of the applied deflection and the original length of the model. True strain is thereafter calculated from the relation $\varepsilon_{true} = \ln(1+\varepsilon_{engineering})$.

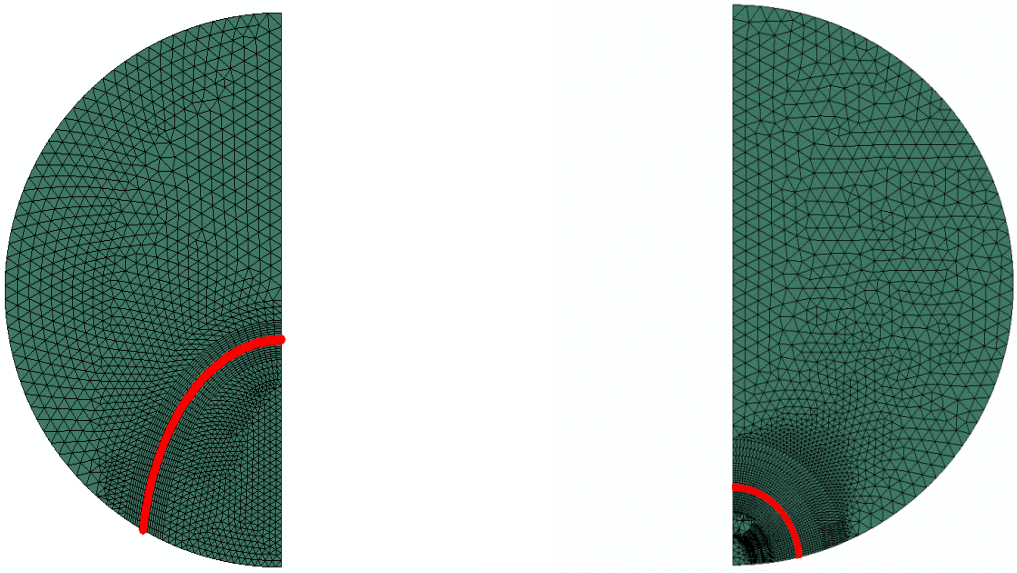

Crack front for defect 1 (test specimen 1). Crack front for defect 2 (test specimen 2).

Figure 6-6. Crack fronts for the two defects considered in this FE-simulation.

The following plots show *J*-values along the crack front (for different values of applied true strain). In Fig. 6-7 the results are presented for defect 1 (the large defect) and in Fig. 6-8 the results are presented for defect 2 (the medium sized defect).

Then follows plots that show the maximum *J*-values, somewhere along the crack front, as a function of true strain. For each defect three plots are presented (see Fig. 6-9 to 6-10):

i) First plot shows the maximum *J*-values as a function of true strain.

ii) Then, the values from the FE-simulation are plotted in stress-strain curve for a BWR-insert material.

iii) Finally, the fracture toughness values (using J_{Ic} and J_{2mm}) are introduced in the stress-strain curve for a BWR-insert material.

- First the strain value equal to $J = J_{Ic}$ (or $J = J_{2mm}$) is taken from plot i).
- An equivalent stress value is then taken from plot ii).
- This stress and strain value is finally introduced in plot iii).

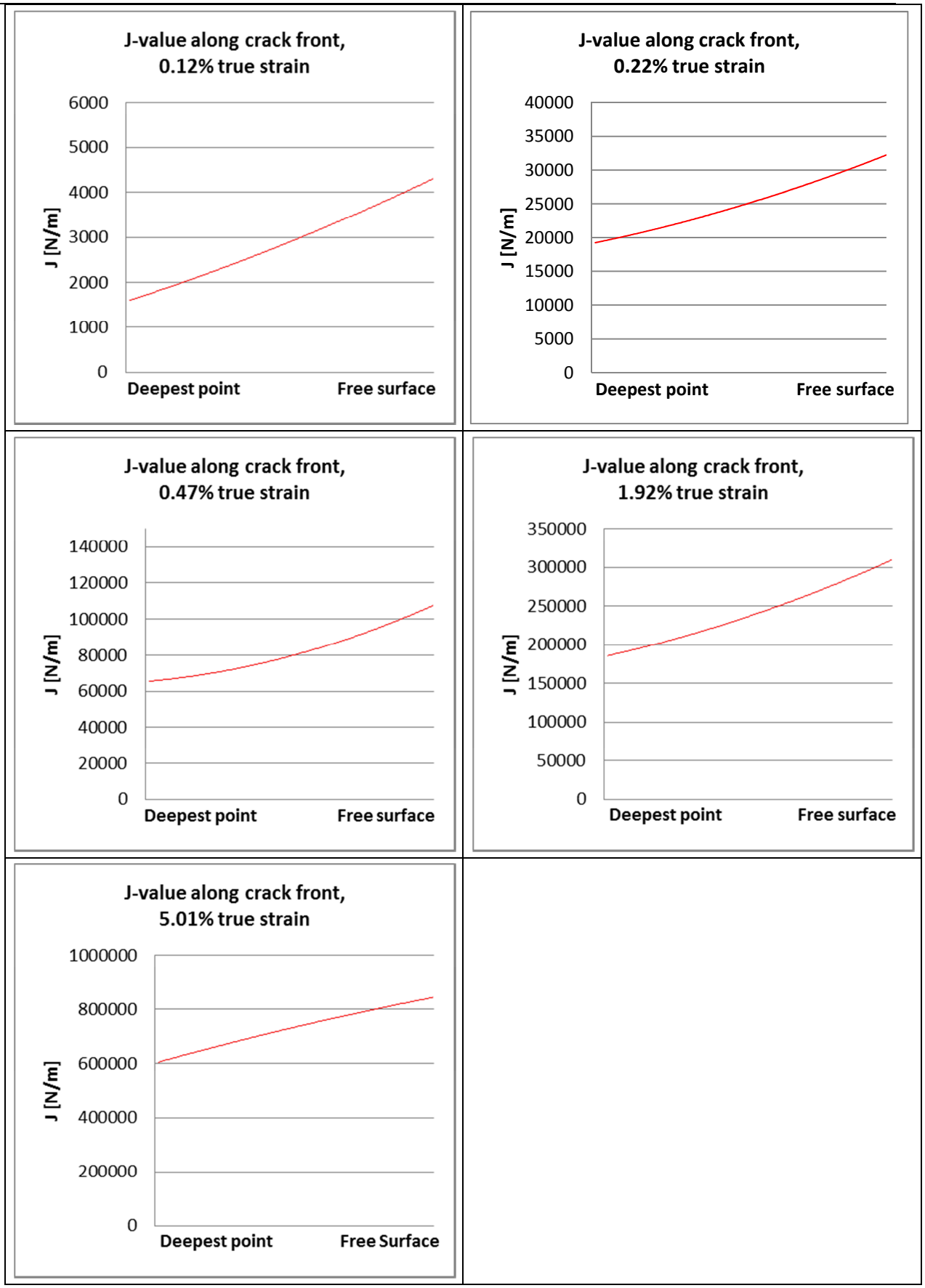

Figure 6-7. *J*-values along the crack front, for defect 1 (for different values of applied true strain).

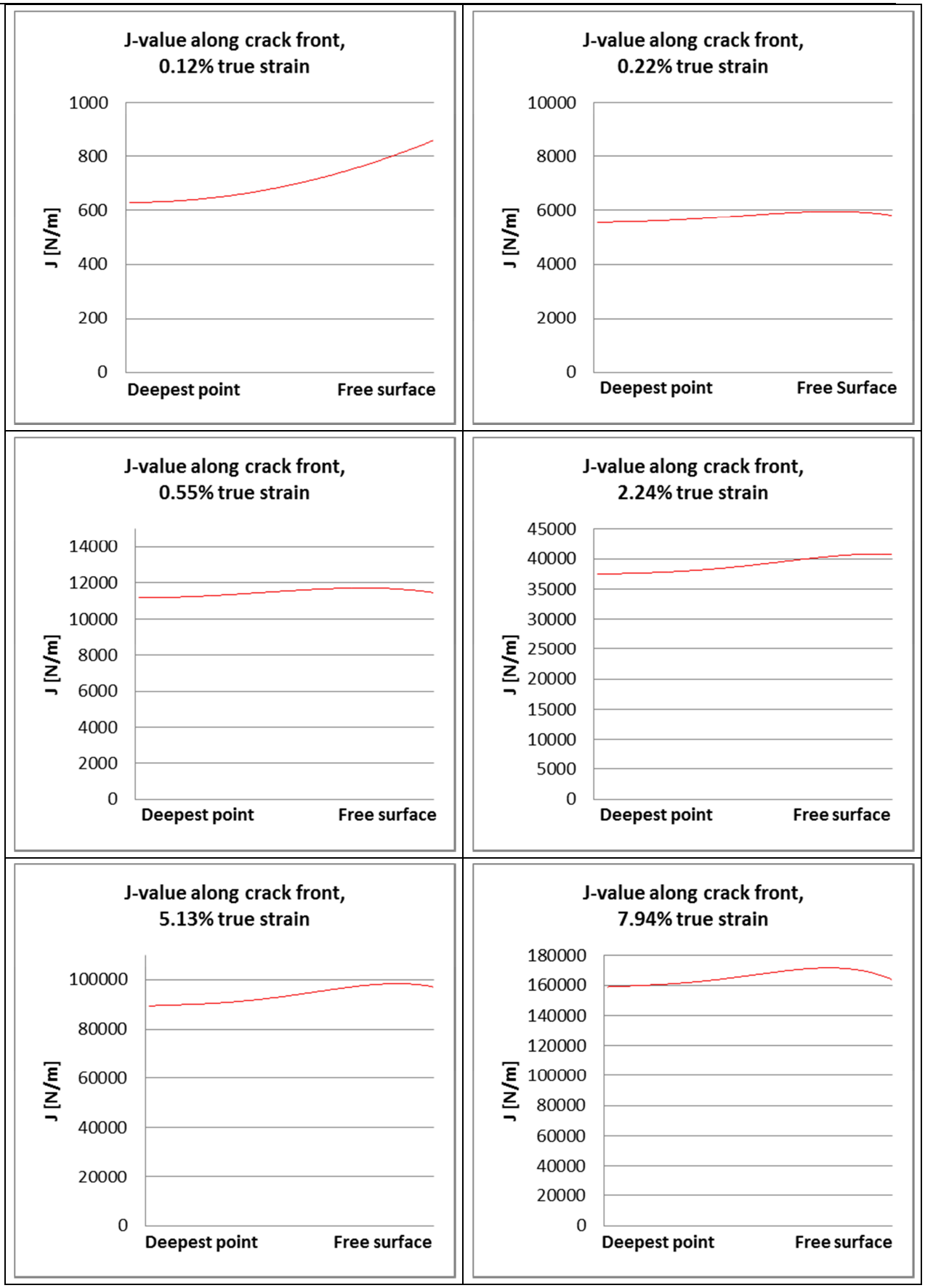

Figure 6-8. *J*-values along the crack front, for defect 2 (for different values of applied true strain).

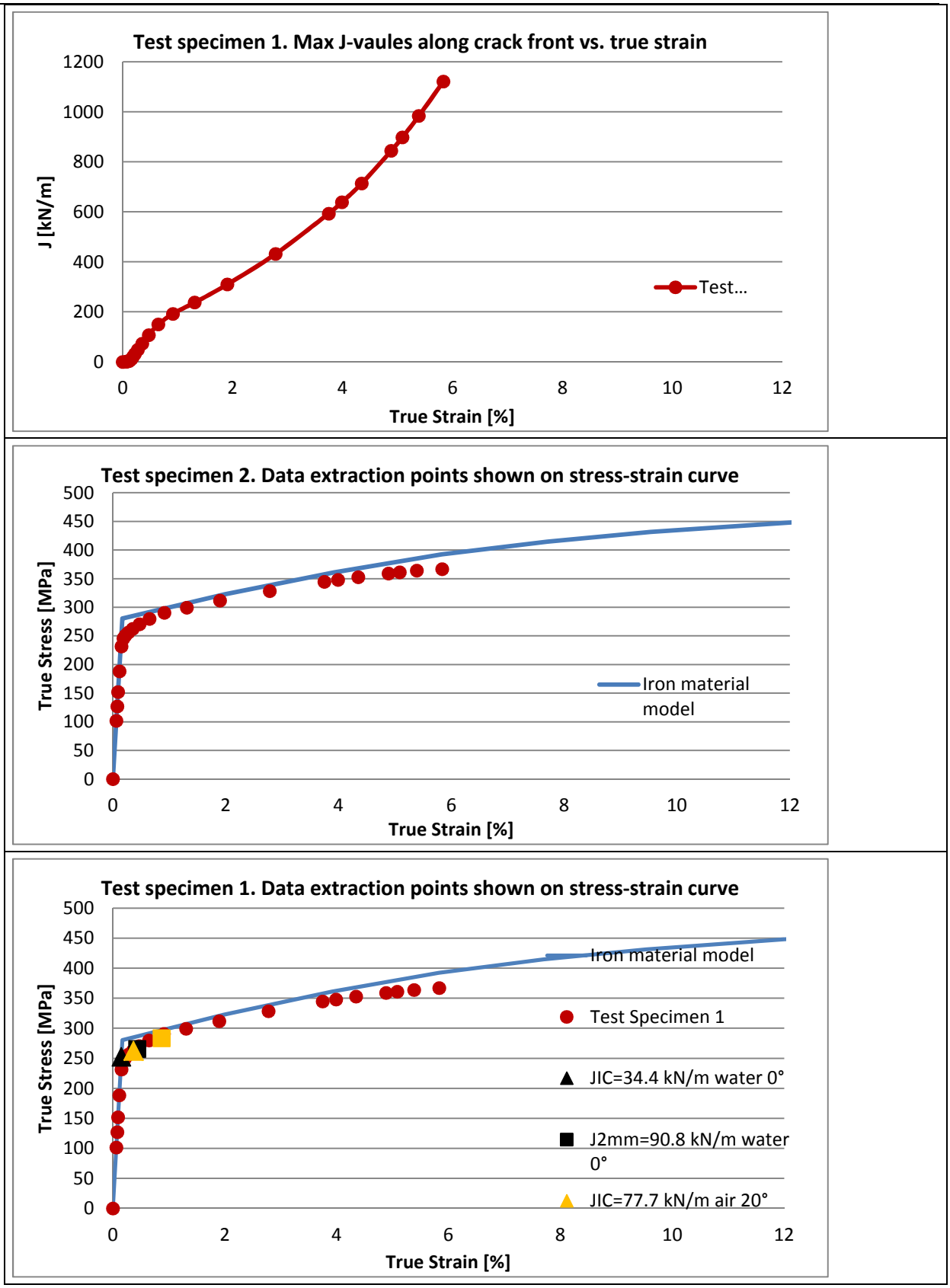

Figure 6-9. Results from FE-simulation of defect 1/test specimen 1 (the maximum *J*-values as a function of true strain and the values from the FE-simulation are plotted in stress-strain curve, including fracture toughness values).

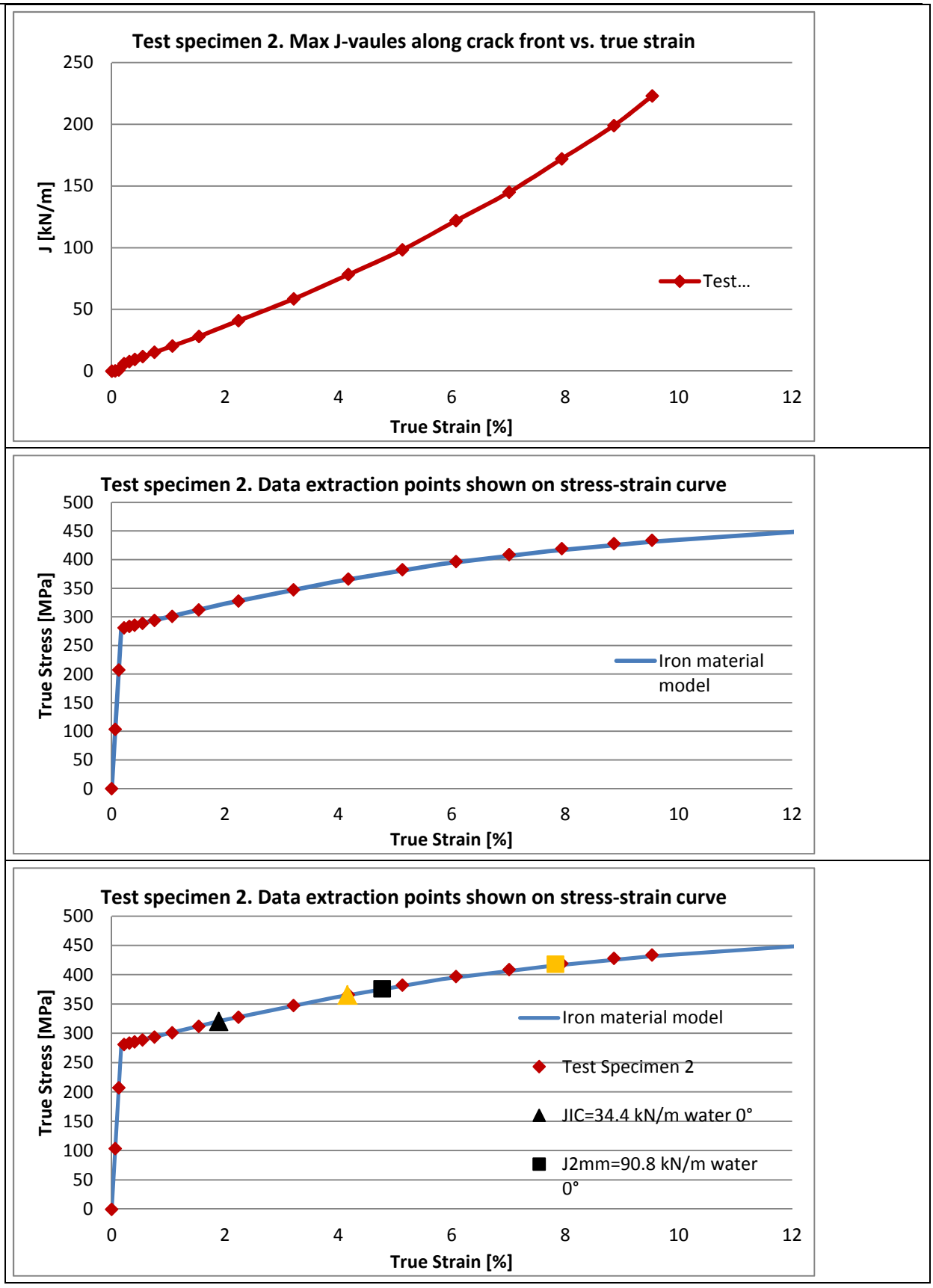

Figure 6-10. Results from FE-simulation of defect 2/test specimen 2 (the maximum *J*-values as a function of true strain and the values from the FE-simulation are plotted in stress-strain curve, including fracture toughness values).

As can be seen in Fig. 6-7 to 6-8, the *J*-values for defect 1 (the large defect) are much higher than the *J*-values from defect 2 (also highlighted in Fig. 6-11). This is reasonable given the difference in size between the two defects.

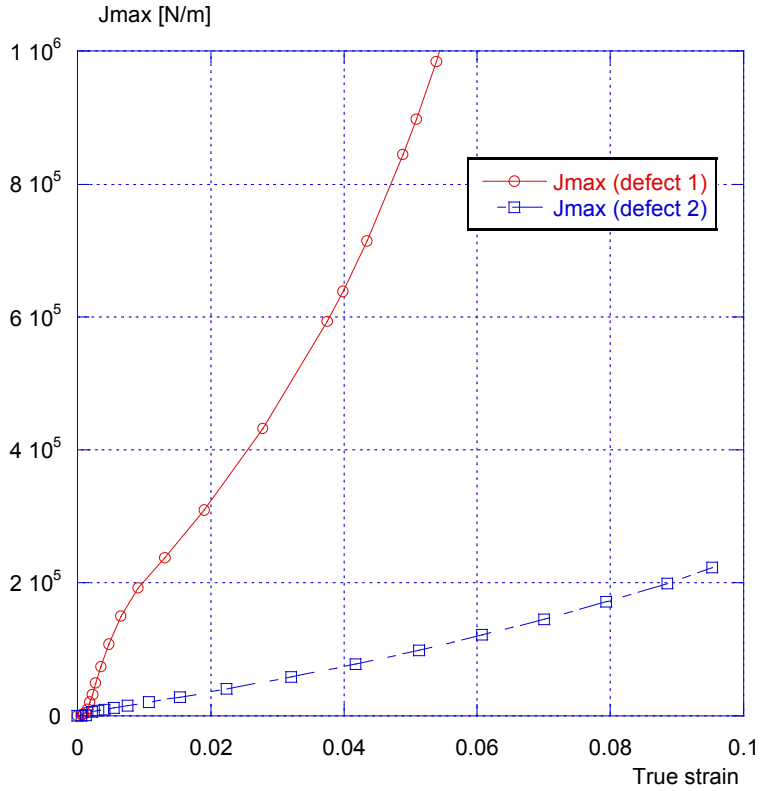

Figure 6-11. The maximum *J*-values, somewhere along the crack front, as a function of true strain (a comparison between defect 1 and 2).

In order to check the accuracy of the FE-simulation a comparison was made using ProSACC. The comparison, using defect 2, is presented in Fig. 6-12.

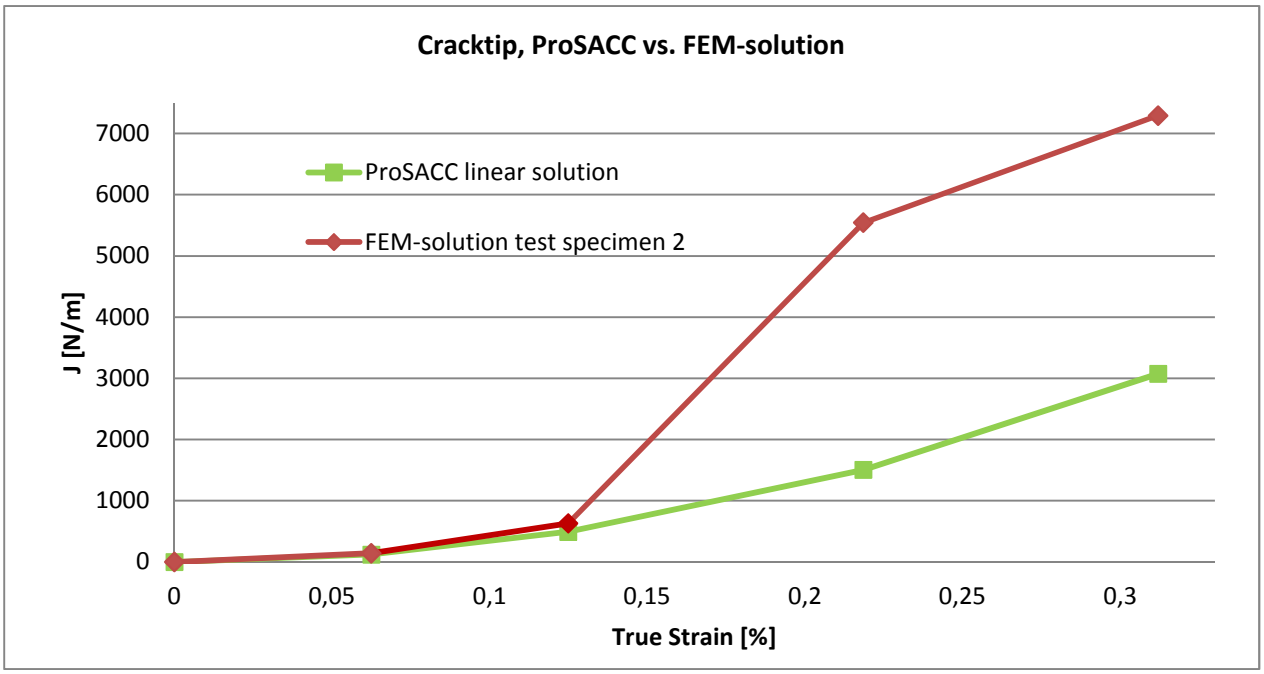

Figure 6-12. Comparison between the FE-simulation and the software ProSACC (using defect 2/test specimen 2).

ProSACC uses a linear solution to calculate *K* (or *J*-values) so it should be a good agreement in the beginning of the analysis. As can be seen in Fig. 6-12, the agreement is very good when you have almost no plasticity in the FE-analysis.

In Fig. 6-9 to 6-10, a comparison is made between the applied *J*-values and the fracture toughness values plotted in a stress strain curve for the insert material. The comparison is made using the following fracture toughness values:

- J_{Ic} = 34.4 kN/m, which is the fracture toughness at initiation of crack growth for a BWR-insert material (tested in water at 0°C) [13].
- J_{2mm} = 90.8 kN/m, which is the fracture toughness at 2mm of stable crack growth for a BWR-insert material (tested in water at 0°C) [13].
- J_{Ic} = 77.7 kN/m, which is the fracture toughness at initiation of crack growth for the PWR-insert IP24, middle section (tested in air at 20°C) [14].
- J_{2mm} = 168.3 kN/m, which is the fracture toughness at 2mm of stable crack growth for the PWR-insert IP24, middle section (tested in air at 20°C) [14].

The PWR-data is chosen to represent the best achievable data at the moment and also tested in air which is considered more relevant than tests conducted in water.

The data for defect 2 (see Fig. 6-10) follows the stress strain curve and a comparison shows that the fracture toughness values are reasonably located on the stress strain curve. For this defect, the assumption of a crack like defect seems to be valid.

The data for defect 1 (see Fig. 6-9) follows the stress strain curve, but not as close as defect 2 and a comparison shows that the fracture toughness values are located too early on the stress strain curve. This indicates that for this larger defect the assumption of a crack-like defect is too conservative and the main reason is probably when treating three small defects as one large defect. For this defect, the stiffness behavior of the FE-simulation did not follow the actual tensile test. It is possible to get a better agreement if one model the three defects in a new FE-model (instead of one large defect).

7 CONCLUSIONS

In this report, defect distributions are developed and documented, for both BWR- and PWR-inserts. These distributions can be used in a probabilistic analysis.

There is a distinct difference between the crack-like defects that are found in BWR- and PWR-inserts. The defects found in PWR-inserts are much smaller (mean value = 0.8 mm) than the defects found in BWR-inserts (mean value = 1.2 mm). Also, there are no outliers in the data set from the PWR-inserts.

An analysis was performed to check whether the assumption, that the found defects are to be treated as crack-like defects, is pessimistic or not. The analysis showed that when it is a good agreement between the analyzed defect and the real defect then the assumption of a crack like defect seems to be valid. However, when it is a large difference between the analyzed defect and the real defect then the assumption of a crack like defect seems to be very pessimistic.

8 LIST OF REFERENCES

[1] DILLSTRÖM, P., et. al., (2008), "A combined deterministic and probabilistic procedure for safety assessment of components with cracks – Handbook", SSM Research Report 2008:01, Swedish Radiation Safety Authority.

[2] DILLSTRÖM, P., and ALVERLIND, L., (2013-12), "Probabilistic analysis of BWR canister inserts for spent nuclear fuel in the case of an earthquake induced rock shear load", Technical Report 50014130-1, Rev. 1, Inspecta Technology AB, SKBdoc 1412158 - ver 1.0.

[3] DILLSTRÖM, P., (2005-10), "Probabilistic analysis of canister inserts for spent nuclear fuel", SKB Technical Report TR-05-19, Swedish Nuclear Fuel and Waste Management Co.

[4] FOURLAKIDIS, V., (2012-08-22), Investigation report 20459 I TOP, Swerea SWECAST AB, SKBdoc 1356755 - ver 1.0.

[5] FOURLAKIDIS, V., (2012-08-22), Investigation report 20458, Swerea SWECAST AB, SKBdoc 1356630 - ver 1.0.

[6] FOURLAKIDIS, V., (2012-08-22), Investigation report 20459-II-BOTTOM, Swerea SWECAST AB, SKBdoc 1356753 - ver 1.0.

[7] FOURLAKIDIS, V., (2012-10-25), Investigation report 20459 I TOP, Issue 3, Swerea SWECAST AB, SKBdoc 1356755 - ver 3.0.

[8] FOURLAKIDIS, V., (2012-10-25), Investigation report 20458, Issue 2, Swerea SWECAST AB, SKBdoc 1356630 - ver 2.0.

[9] FOURLAKIDIS, V., (2012-10-25), Investigation report 20459-II-BOTTOM, Issue 2, Swerea SWECAST AB, SKBdoc 1356753 - ver 2.0.

[10] FOURLAKIDIS, V., (2013-10-25), Investigation report 20587, Issue 2, Swerea SWECAST AB, SKBdoc 1404899 - ver 1.0.

[11] FOURLAKIDIS, V., (2013-10-25), Investigation report 20588, Issue 2, Swerea SWECAST AB, SKBdoc 1405581 - ver 1.0.

[12] FOURLAKIDIS, V., (2013-10-25), Investigation report 20556, Issue 2, Swerea SWECAST AB, SKBdoc 1398186 - ver 2.0.

[13] DILLSTRÖM, P. and BOLINDER, T., (2010-10), "Damage tolerance analysis of canister inserts for spent nuclear fuel in the case of an earthquake induced rock shear load", SKB Technical Report TR-10-29, Swedish Nuclear Fuel and Waste Management Co.

[14] SHIPSHA, A., (2013-12-03), "Statistical data analysis of cast iron properties for PWR-inserts from tension, compression and fracture toughness testing", Technical Report 50017490-1, Rev. 1, Inspecta Technology AB, SKBdoc 1414800 - ver 1.0.

9 REVISIONS

Rev	Reason for change/Pages or chapters	Our reference	Date
0	—	Peter Dillström	2013-12-04
1	The report is revised according to the review comments in SKBDoc 1418819, Ver. 0.5.	Peter Dillström	2014-02-16
2	The report is revised according to the review comments in SKBDoc 1430060, Ver. 0.2.	Peter Dillström	2014-02-27

10 APPENDIX A. DATA FROM FRACTURE SURFACES ON TENSILE TEST SPECIMENS (BWR INSERTS)

On each fracture surface, and for each defect found on that surface, the following information was summarized:

- Test specimen number (given as a combination of sample and bar number).
- Type of defect (porosity defects and graphite/dross defects) on that surface. The graphite/dross defects should be included when developing a new defect distribution for crack-like defects (only graphite/dross defects are included in the table below).
- Area of defect (the real defect was first manually marked by using a photo manipulation tool and then an image analysis software was used to measure the exact area of the defect, see Fig. 2-1).
- Area of ellipse (drawn surrounding the real defect, see Fig. 2-1).
- Major and minor axis of the ellipse (see Fig. 2-1). The minor axis of the ellipse is equal to the defect depth and the major axis is equal to the defect length.

Also included in the table is the elongation at fracture for each tensile test specimen.

Sample	Bar No	Defects area [mm^2]	Ellipse area [mm^2]	Major axis [mm]	Minor axis [mm]	Elongation at fracture
I53M	1	3.63	3.78	2.66	1.8	14.7
I53M	2	0.25	0.27	0.76	0.44	18.7
I53M	3	0.3	0.33	0.68	0.62	17.7
I53M	4	2.65	2.89	1.96	1.88	14.9
I53M	5	1.2	1.3	1.7	1	17.6
I53M	5	0.48	0.5	1.1	0.6	17.6
I54M	2	3.44	3.77	2.4	2	15.4
I54M	3	1.09	2.64	3.12	1.08	19.4
I54M	4	0.63	0.6	1.1	0.7	15.9
I54M	5	3.61	6.86	3.88	2.46	14.6
I54M	5	2.51	3.31	2.3	1.84	14.6
I54M	5	5.2	9.34	4.14	2.86	14.6
I55M	2	0.91	1.46	1.54	1.2	18.1
I55M	3	1.21	2.07	2.2	1.22	14.3
I55M	3	2.56	4.98	2.6	2.44	14.3
I55M	3	0.3	0.36	0.74	0.62	14.3
I55M	4	1.69	1.85	1.66	1.42	15.6
I55M	4	0.76	1.2	1.78	0.86	15.6
I55M	6	1.48	1.57	2	1	15.1
I55M	6	0.85	0.99	1.8	0.7	15.1

Sample	Bar No	Defects area [mm^2]	Ellipse area [mm^2]	Major axis [mm]	Minor axis [mm]	Elongation at fracture
I56M	2	1.91	3.84	2.4	1.64	15.3
I56M	3	1.37	1.49	1.66	1.14	14.9
I56M	4	1.6	3	2.66	1.44	16.9
I56M	4	0.97	2.03	2	1.3	16.9
I56M	5	2.38	2.5	2.76	1.16	13.3
I53T	2	0.14	0.23	0.66	0.44	18.1
I53T	3	3.08	3.54	3.06	1.48	14.7
I53T	3	1.04	1.33	1.76	0.96	14.7
I53T	4	6.27	7.47	4.52	2.1	8.9
I53T	5	1.45	2.53	2.06	1.56	17.6
I53T	6	0.9	0.93	1.36	0.86	13.1
I53T	6	3.08	5.76	9.62	5.56	13.1
I53T	6	0.5	0.52	0.86	0.76	13.1
I54T	1	1.86	1.84	1.96	1.2	7.6
I54T	1	3.11	3.13	2.1	1.9	7.6
I54T	4	8.32	31.64	8.18	5.72	9
I54T	4	1.98	1.93	2.88	2.68	9
I54T	5	2.94	7.5	3.32	2.88	9.1
I54T	5	3.24	5.4	2.8	2.46	9.1
I54T	5	1.38	2.81	1.9	1.88	9.1
I54T	6	1.52	6.5	3.4	2.44	11.7
I54T	6	1.01	1.28	1.56	1.04	11.7
I54T	6	2.48	2.34	1.98	1.5	11.7
I55T	1	0.71	0.98	1.32	0.94	13.4
I55T	1	1.12	4.08	3.16	1.64	13.4
I55T	2	1.34	1.87	1.84	1.3	14.7
I55T	2	1.37	1.96	2.46	1.02	14.7
I55T	4	0.34	0.32	1.1	0.36	17.7
I55T	6	0.18	0.28	0.64	0.56	20
I56T	1	0.22	0.23	0.76	0.38	13.1
I56T	1	1.54	2.18	1.7	1.64	13.1
I56T	1	4.94	5.1	11.72	6.8	13.1
I56T	1	0.13	0.2	0.078	0.32	13.1

Sample	Bar No	Defects area [mm^2]	Ellipse area [mm^2]	Major axis [mm]	Minor axis [mm]	Elongation at fracture
I56T	2	0.17	0.19	0.6	0.4	17.7
I56T	3	3.51	5.97	4.34	1.76	12
I56T	3	0.47	0.52	0.9	0.74	12
I56T	4	7.13	7.66	3.54	2.76	7.6
I56T	4	1.01	1.05	1.72	0.78	7.6
I56T	4	9.13	11.73	4.56	3.28	7.6
I56T	5	2.16	2.39	2.42	1.26	17.9
I56T	5	0.97	0.95	1.64	0.74	17.9
I57T	1	4.37	7.06	4.68	1.92	12.1
I57T	2	0.73	0.78	1.04	0.96	7.3
I57T	3	2.38	2.57	2	1.64	12.3
I57T	3	1.44	1.57	2	1	12.3
I57T	3	0.16	0.24	0.74	0.42	12.3
I57T	3	1.72	1.86	1.82	1.3	12.3
I57T	4	0.22	0.22	0.72	0.38	11
I57T	4	7.94	13.72	6.64	2.64	11
I57T	6	1.04	1.06	1.26	1.08	16.4
I57T	6	0.67	0.72	1.1	0.82	16.4
I53B	1	0.15	0.16	0.92	0.22	18
I53B	2	2.1	2.42	2	1.54	17.3
I53B	2	0.23	0.24	0.6	0.5	17.3
I53B	4	0.48	0.86	1.5	0.72	17.7
I53B	4	0.13	0.13	0.48	0.3	17.7
I53B	5	0.17	0.32	0.9	0.46	15.9
I53B	5	0.98	1.12	1.74	0.82	15.9
I53B	5	0.24	0.55	1.32	0.52	15.9
I53B	5	0.16	0.38	1.5	0.32	15.9
I53B	5	0.5	0.61	0.96	0.8	15.9
I53B	5	0.29	0.31	0.88	0.44	15.9
I53B	6	0.01	0.01	0.42	0.3	19
I54B	4	0.66	0.68	1.14	0.76	14
I54B	4	0.19	0.3	0.8	0.48	14

Sample	Bar No	Defects area [mm^2]	Ellipse area [mm^2]	Major axis [mm]	Minor axis [mm]	Elongation at fracture
I55B	6	1.64	3.57	2.78	1.64	13.3
I55B	6	0.98	1.16	1.94	0.76	13.3
I55B	6	0.43	0.43	0.78	0.7	13.3
I56B	2	0.37	0.4	0.76	0.66	18.7
I56B	3	0.75	0.77	1.38	0.7	18.1
I56B	4	0.55	0.6	0.9	0.84	18.9
I56B	4	0.23	0.31	0.86	0.46	18.9
I56B	4	0.96	1.06	1.3	1.04	18.9
I56B	4	0.7	0.8	1.04	0.98	18.9
I56B	5	1.22	1.28	1.56	1.04	16.1
I56B	5	0.71	0.92	1.6	0.74	16.1
I56B	6	0.2	0.3	0.88	0.44	14
I56B	6	0.68	0.77	1.4	0.7	14
I57B	2	0.55	0.55	0.98	0.72	18
I57B	5	0.75	1.28	1.84	0.88	19.9

11 APPENDIX B. CORRECTED DATA FROM FRACTURE SURFACES ON TENSILE TEST SPECIMENS (BWR INSERTS)

On each fracture surface, and for each defect found on that surface, the following information was summarized:

- Test specimen number (given as a combination of sample and bar number).
- Type of defect (porosity defects and graphite/dross defects) on that surface. The graphite/dross defects should be included when developing a new defect distribution for crack-like defects (only graphite/dross defects are included in the table below).
- Area of defect (the real defect was first manually marked by using a photo manipulation tool and then an image analysis software was used to measure the exact area of the defect, see Fig. 2-1).
- Area of ellipse (drawn surrounding the real defect, see Fig. 2-1).
- Major and minor axis of the ellipse (see Fig. 2-1). The minor axis of the ellipse is equal to the defect depth and the major axis is equal to the defect length.

Also included in the table is the elongation at fracture for each tensile test specimen.

Sample	Bar No	Defects area [mm^2]	Ellipse area [mm^2]	Major axis [mm]	Minor axis [mm]	Elongation at fracture
I53M	1	3.63	3.76	2.66	1.8	14.7
I53M	2	0.25	0.26	0.76	0.44	18.7
I53M	3	0.3	0.33	0.68	0.62	17.7
I53M	4	2.65	2.89	1.96	1.88	14.9
I53M	5	1.2	1.33	1.7	1	17.6
I53M	5	0.48	0.52	1.1	0.6	17.6
I54M	2	3.44	3.77	2.4	2	15.4
I54M	3	1.09	2.65	3.12	1.08	19.4
I54M	4	0.6	0.6	1.1	0.7	15.9
I54M	5	3.61	6.88	3.88	2.26	14.6
I54M	5	2.51	3.32	2.3	1.84	14.6
I54M	5	5.2	9.29	4.14	2.86	14.6
I55M	2	0.91	1.45	1.54	1.2	18.1
I55M	3	1.21	2.11	2.2	1.22	14.3
I55M	3	2.56	4.98	2.6	2.44	14.3
I55M	3	0.3	0.36	0.74	0.62	14.3
I55M	4	1.69	1.85	1.66	1.42	15.6
I55M	4	0.76	1.2	1.78	0.86	15.6
I55M	6	1.48	1.57	2	1	15.1
I55M	6	0.85	0.99	1.8	0.7	15.1

Sample	Bar No	Defects area [mm^2]	Ellipse area [mm^2]	Major axis [mm]	Minor axis [mm]	Elongation at fracture
I56M	2	1.91	3.09	2.4	1.64	15.3
I56M	3	1.37	1.49	1.66	1.14	14.9
I56M	4	1.6	3.01	2.66	1.44	16.9
I56M	4	0.97	2.04	2	1.3	16.9
I56M	5	2.38	2.51	2.76	1.16	13.3
I53T	2	0.14	0.23	0.66	0.44	18.1
I53T	3	3.08	3.56	3.06	1.48	14.7
I53T	3	1.04	1.33	1.76	0.96	14.7
I53T	4	6.27	7.45	4.52	2.1	8.9
I53T	5	1.45	2.52	2.06	1.56	17.6
I53T	6	0.9	0.92	1.36	0.86	13.1
I53T	6	3.08	5.77	3.6	2.04	13.1
I53T	6	0.5	0.51	0.86	0.76	13.1
I54T	1	1.86	1.85	1.96	1.2	7.6
I54T	1	3.11	3.13	2.1	1.9	7.6
I54T	4	3.31	5.99	2.86	2.66	9
I54T	4	15.84	31.95	7.1	5.74	9
I54T	5	2.94	7.51	3.32	2.88	9.1
I54T	5	3.24	5.41	2.8	2.46	9.1
I54T	5	1.38	2.8	1.9	1.88	9.1
I54T	6	1.52	6.51	3.4	2.44	11.7
I54T	6	1.01	1.27	1.56	1.04	11.7
I54T	6	2.48	2.48	2.00	1.58	11.7
I55T	1	0.71	0.97	1.32	0.94	13.4
I55T	1	1.12	4.07	3.16	1.64	13.4
I55T	2	1.34	1.88	1.84	1.3	14.7
I55T	2	1.37	1.97	2.46	1.02	14.7
I55T	4	0.34	0.35	1.16	0.38	17.7
I55T	6	0.18	0.28	0.64	0.56	20
I56T	1	0.22	0.23	0.76	0.38	13.1
I56T	1	1.54	2.19	1.7	1.64	13.1
I56T	1	4.94	5.09	3.34	1.94	13.1
I56T	1	0.13	0.2	0.78	0.32	13.1

Sample	Bar No	Defects area [mm^2]	Ellipse area [mm^2]	Major axis [mm]	Minor axis [mm]	Elongation at fracture
I56T	2	0.17	0.19	0.6	0.4	17.7
I56T	3	3.51	6.0	4.34	1.76	12
I56T	3	0.47	0.52	0.9	0.74	12
I56T	4	7.13	7.67	3.54	2.76	7.6
I56T	4	1.01	1.05	1.72	0.78	7.6
I56T	4	9.13	11.74	4.56	3.28	7.6
I56T	5	2.16	2.39	2.42	1.26	17.9
I56T	5	0.97	0.95	1.64	0.74	17.9
I57T	1	4.37	7.05	4.68	1.92	12.1
I57T	2	0.73	0.78	1.04	0.96	7.3
I57T	3	2.38	2.57	2	1.64	12.3
I57T	3	1.44	1.57	2	1	12.3
I57T	3	0.16	0.24	0.74	0.42	12.3
I57T	3	1.72	1.86	1.82	1.3	12.3
I57T	4	0.22	0.21	0.72	0.38	11
I57T	4	7.94	13.76	6.64	2.64	11
I57T	6	1.04	1.07	1.26	1.08	16.4
I57T	6	0.67	0.71	1.1	0.82	16.4
I53B	1	0.15	0.16	0.92	0.22	18
I53B	2	2.1	2.42	2	1.54	17.3
I53B	2	0.23	0.24	0.6	0.5	17.3
I53B	4	0.48	0.85	1.5	0.72	17.7
I53B	4	0.13	0.13	0.5	0.32	17.7
I53B	5	0.17	0.32	0.9	0.46	15.9
I53B	5	0.98	1.12	1.74	0.82	15.9
I53B	5	0.24	0.54	1.32	0.52	15.9
I53B	5	0.16	0.38	1.5	0.32	15.9
I53B	5	0.5	0.6	0.96	0.8	15.9
I53B	5	0.29	0.3	0.88	0.44	15.9
I53B	6	0.06	0.1	0.42	0.3	19
I54B	4	0.66	0.68	1.14	0.76	14
I54B	4	0.19	0.3	0.8	0.48	14

Sample	Bar No	Defects area [mm^2]	Ellipse area [mm^2]	Major axis [mm]	Minor axis [mm]	Elongation at fracture
I55B	6	1.64	3.57	2.78	1.64	13.3
I55B	6	0.98	1.16	1.94	0.76	13.3
I55B	6	0.43	0.43	0.78	0.7	13.3
I56B	2	0.37	0.4	0.76	0.66	18.7
I56B	3	0.75	0.77	1.38	0.7	18.1
I56B	4	0.55	0.6	0.9	0.84	18.9
I56B	4	0.23	0.31	0.86	0.46	18.9
I56B	4	0.96	1.06	1.3	1.04	18.9
I56B	4	0.7	0.8	1.04	0.98	18.9
I56B	5	1.22	1.28	1.56	1.04	16.1
I56B	5	0.71	0.92	1.6	0.74	16.1
I56B	6	0.2	0.3	0.88	0.44	14
I56B	6	0.68	0.77	1.4	0.7	14
I57B	2	0.55	0.55	0.98	0.72	18
I57B	5	0.75	1.28	1.84	0.88	19.9

12 APPENDIX C. DATA FROM FRACTURE SURFACES ON TENSILE TEST SPECIMENS (PWR INSERTS)

On each fracture surface, and for each defect found on that surface, the following information was summarized:

- Test specimen number (given as a combination of sample and bar number).
- Type of defect (porosity defects and graphite/dross defects) on that surface. The graphite/dross defects should be included when developing a new defect distribution for crack-like defects (only graphite/dross defects are included in the table below).
- Area of defect (the real defect was first manually marked by using a photo manipulation tool and then an image analysis software was used to measure the exact area of the defect, see Fig. 2-1).
- Area of ellipse (drawn surrounding the real defect, see Fig. 2-1).
- Major and minor axis of the ellipse (see Fig. 2-1). The minor axis of the ellipse is equal to the defect depth and the major axis is equal to the defect length.

Also included in the table is the elongation at fracture for each tensile test specimen.

Sample	Bar No	Defects area [mm^2]	Ellipse area [mm^2]	Major axis [mm]	Minor axis [mm]	Elongation at fracture
IP23B	3	0.09	0.1	0.4	0.3	20.5
IP23B	3	0.13	0.14	0.66	0.28	20.5
IP23B	7	0.81	1.35	2.68	0.64	21.4
IP23B	8	0.8	1.88	2.78	0.86	18.2
IP23M	7	2.21	2.21	2.34	1.2	10.2
IP23T	3	0.52	0.59	1.22	0.62	19.3
IP24B	3	0.58	0.6	1	0.76	20.3
IP24B	5	0.33	0.47	0.82	0.74	19
IP24B	7	0.74	0.75	1.1	0.86	20.8
IP24B	7	0.6	0.85	1.08	1	20.8
IP24B	7	0.54	1.47	1.86	1	20.8
IP24B	8	0.44	0.55	1.5	0.46	20.5
IP24M	4	0.86	0.86	1.86	0.6	14.3
IP24M	6	0.72	1.72	2.44	0.9	21.1
IP24M	7	0.44	0.44	0.76	0.74	11.9
IP24M	7	0.84	0.85	1.42	0.76	11.9
IP24M	7	2.43	4.11	3.1	1.7	11.9
IP24T	1	0.27	0.28	0.8	0.44	22
IP24T	2	1.42	1.49	2.02	0.94	18.7
IP24T	2	0.29	0.34	0.9	0.48	18.7

Sample	Bar No	Defects area [mm^2]	Ellipse area [mm^2]	Major axis [mm]	Minor axis [mm]	Elongation at fracture
IP24T	3	0.48	0.51	0.92	0.7	14.6
IP24T	3	0.85	1.34	2.1	0.82	14.6
IP24T	4	1.92	2.27	2.32	1.26	12.3
IP24T	4	2.32	2.64	4.2	0.8	12.3
IP24T	8	0.31	0.38	1.14	0.42	18.1
IP24T	8	1.18	1.87	2.54	0.94	18.1
IP25B	2	0.3	0.42	0.96	0.56	17.6
IP25B	2	1.34	1.8	2.4	0.96	17.6
IP25B	5	0.42	0.5	0.98	0.64	17.4
IP25M	1	0.19	0.19	0.68	0.36	13.6
IP25M	4	1.01	1.32	1.42	1.18	9.4
IP25M	7	1.58	2.09	2.6	1.02	8
IP25M	7	2.23	3.58	2.66	1.72	8
IP25M	7	0.82	1.13	1.72	0.84	8
IP25M	7	0.81	1.93	1.74	1.42	8
IP25M	7	0.57	0.58	1.06	0.7	8
IP25T	2	0.1	0.14	0.42	0.42	14.1
IP25T	3	0.54	1.41	2	0.9	10.5
IP25T	3	0.36	0.46	1.04	0.56	10.5
IP25T	3	0.38	0.59	1.16	0.64	10.5